2.5 Department of Theory

Director:

Walter Thiel (born 1949)

Further group leaders:

Mario Barbatti (born 1972)

Elsa Sánchez-García (born 1976)

Curriculum Vitae: Walter Thiel

1949	Born in Treysa, Germany
1966-1971	Chemistry studies at Universität Marburg
1971-1973	Doctoral studies at Universität Marburg, with A. Schweig
1973-1975	Postdoctoral fellow at the University of Texas at Austin, with M. J. S. Dewar
1975-1982	Research scientist at Universität Marburg
1981	Habilitation for Theoretical Chemistry
1983-1992	Associate Professor of Theoretical Chemistry at Universität Wuppertal
1987	Guest Professor at the University of California at Berkeley
1992-1999	Full Professor of Chemistry at Universität Zürich
1999	Director at the Max-Planck-Institut für Kohlenforschung in Mülheim/Ruhr
2001	Honorary Professor at Universität Düsseldorf

Awards and Honors

1969-1974	Studienstiftung des deutschen Volkes
1975-1977	Liebig Fellowship, Verband der Chemischen Industrie
1982	Heisenberg Fellowship, Deutsche Forschungsgemeinschaft
1988	Förderpreis, Alfried-Krupp Stiftung
1991	Member, European Academy of Sciences and Arts
2002	Schrödinger Medal, World Association of Theoretical Chemists
2007	Member, Deutsche Akademie der Naturforscher Leopoldina
2007	Member, International Academy of Quantum Molecular Sciences
2008	Member, Nordrhein-Westfälische Akademie der Wissenschaften
2009	Festschrift, Journal of Physical Chemistry A 2009, 113 (43), 11455-12044
2012	Liebig Medal, German Chemical Society
2013	ERC Advanced Grant, European Research Council

Special Activities

1986-1992	Member of the Board, Institut für Angewandte Informatik, Wuppertal
1990-1992	Speaker, DFG-Forschergruppe: Reaktive Moleküle
1997-	Advisory Editor, Theoretical Chemistry Accounts
1998-	Advisory Editor, Journal of Computational Chemistry
2000-2008	Reviewer (Fachkollegiat), Deutsche Forschungsgemeinschaft
2000-2006	Member of the Board (Lenkungsausschuss), Bavarian Supercomputer Center (Höchstleistungsrechenzentrum Bayern)

2001-2005	Chairman, Arbeitsgemeinschaft Theoretische Chemie
2002-2008	Section Editor, Encyclopedia of Computational Chemistry
2004-2007	Member, Ständiger Ausschuss der Bunsengesellschaft
2004-	Member of the Scientific Advisory Board, Lise Meitner Minerva Center for Quantum Chemistry, Jerusalem/Haifa, Israel
2006-2008	Managing Director, Max-Planck-Institut für Kohlenforschung
2006-2012	Chairman, BAR Committee of the Max Planck Society
2006-2013	Member of the Kuratorium, Angewandte Chemie
2008-	Associate Editor, WIRES: Computational Molecular Sciences
2009-	Member of the International Advisory Board, State Key Laboratory of Physical Chemistry (PCOSS), Xiamen, China
2010	Chairman, Gordon Conference on Computational Chemistry
2011-	Member of the International Advisory Board, Institute of Organic Chemistry and Biochemistry, Prague, Czech Republic
2011-	President, World Association of Theoretical and Computational Chemists
2012-2013	Editorial Advisory Board, ACS Catalysis
2012-	Editorial Advisory Board, Accounts of Chemical Research
2012-	Member of the Board of Governors, German Chemical Society

Research in the Department of Theory

The Department of Theory comprises the research group of Prof. Walter Thiel and two junior groups headed by PD Dr. Mario Barbatti and Dr. Elsa Sánchez-García.

The central research objectives in the Department are theoretical developments to extend the scope of computational methodology, and applications to study problems of current chemical interest by computation. Such applications are mostly conducted in close cooperation with experimental partners.

In the group of Prof. Thiel, the main field of research is quantum chemistry. Methodological developments and chemical applications are considered to be of equal importance. The research interests range from accurate and almost quantitative calculations on small molecules to the approximate modeling of very large molecules.

The activities of the group cover
(a) ab initio methods (e.g., coupled cluster approaches, CCSD(T)),
(b) density functional theory (DFT),
(c) semiempirical methods (MNDO and beyond),
(d) combined quantum mechanical/molecular mechanical methods (QM/MM).

Recent applications in these four areas focus on
(a) vibration-rotation and electronic spectroscopy of small molecules,
(b) catalytic reactions of transition metal compounds,
(c) electronically excited states in large molecules,
(d) reaction mechanisms in enzymes.

The group of Dr. Barbatti uses ab initio and density functional methods to study nonadiabatic processes that occur after molecular photoexcitation. Methodologically, the aim is to implement new methods and algorithms to improve excited-state simulations within the Newton-X platform and to critically assess their quality. Applications include nonadiabatic dynamics simulations of ultrafast photoinduced processes in biologically relevant molecules and in molecular photo-triggers.

The research in the group of Dr. Sánchez-García focuses on molecular interactions in organic and biological systems, in particular on the introduction of ligands capable of altering protein function, on the interaction of proteins with their biological

environment, and on designed mutagenesis for the regulation of enzymatic activity. The code development targets the implementation of coarse-grained force field methods in QM/MM approaches.

Several cooperations between the Department of Theory and the experimental groups in the Institute have been established over the past years. There have been major collaborative projects on gold catalysis (Fürstner, Alcarazo), palladium catalysis (Maulide), platinum catalysis (Alcarazo), organocatalysis (List), enzymatic catalysis (Reetz), and cellulose depolymerization (Rinaldi, Schüth). In continuation of these efforts, there are a number of ongoing joint projects that employ quantum-chemical calculations to unravel the mechanisms of catalytic reactions studied by the experimental groups in the Institute.

More detailed information on the research areas of the Department is available in the following seven individual reports and in the scientific papers published in 2011-2013. It should be noted that, for the sake of brevity, some of these papers have not been discussed in the reports on the research areas of the Department, and should therefore be consulted directly, if necessary.

The overall direction of research in the Department has remained unchanged during the reporting period, with a notable trend to put more emphasis on the study of electronically excited states and of biologically relevant systems. This is also reflected in the research of the two junior groups. For the future, we anticipate that the focus on large complex systems will remain prominent in the research of the Department, both with regard to method development and chemical applications. We expect that the scope of the research activities will continue to be as broad as in the past, but there will also be some shifts and new directions. In the Thiel group, the method development towards improved semiempirical methods will be intensified in the framework of an ERC Advanced Grant (2014-2018), and there will be more emphasis on QM/MM studies of solvent effects on enzymatic reactivity due to the participation in the RESOLV Cluster of Excellence at the University of Bochum (2012-2017) that is dedicated to solvation science. In this context, a third junior research group will be established at our Department in January 2014, which will be headed by Dr. Matthias Heyden, an expert in classical molecular dynamics simulations of solvent phenomena, who has been selected in a thematically open RESOLV competition.

2.5.1 Research area "Ab Initio Methods" (W. Thiel)

Involved: J. Breidung, G. Cui, Y. Lu, A. Owen, I. Polyak, T. Ribeyre, A. Yachmenev

Objective: Vibration-rotation and electronic spectra of small molecules are computed with high accuracy using high-level ab initio calculations with large basis sets. This research includes the further development of a general variational treatment of nuclear motion that allows the accurate prediction of rovibrational energies and intensities. Highly correlated ab initio methods are also applied for validation and benchmark purposes in studies on electronically excited states.

Results: The theoretical prediction of vibration-rotation spectra requires the generation of accurate potential energy and dipole moment surfaces, followed by the variational calculation of rovibrational energies and intensities. For the former task, we employ ab initio electronic structure methods, typically coupled cluster theory with complete basis set (CBS) extrapolation and corrections for core-valence correlation and relativististic effects. For the latter, we have developed and coded a variational treatment of nuclear motion that is based on the Hougen-Bunker-Johns approach with an Eckart-frame kinetic energy operator and thus also handles large amplitude motion. This has led to a general and robust variational code (TROVE) that was published in 2007.

Over the past three years, TROVE has been extended in several ways. An automated procedure has been added that permits the further refinement of ab initio potential energy surfaces against accurate high-resolution experimental data using variational rovibrational calculations [15]. Technical improvements include coverage of additional molecular group symmetries (e.g., $\boldsymbol{T}_d(M)$), extension of the Numerov-Cooley method to allow periodic solutions of the one-dimensional Schrödinger equation (e.g., for torsions), implementation of eigensolvers for very large Hamiltonian matrices (with dimensions greater than 100,000), and more efficient storage strategies. The available functionality was extended towards the calculation of the rovibrational density matrix exponential and temperature corrections to molecular electromagnetic properties as well as partition functions and thermodynamic parameters (unpublished work by A. Yachmenev and S. Yurchenko).

In the reporting period, the TROVE program has been applied to study formaldehyde [7], thioformaldehyde [12, 81], ammonia [71], and methane [76]. The most extensive project was the calculation of a comprehensive line list for thioformaldehyde (^1H_2CS)

covering all rovibrational transitions that involve states up to 5000 cm^{-1} and rotational quantum number J = 30 (547,926 transitions between 41,809 energy levels) [81]. The TROVE computations were based on a six-dimensional potential energy surface determined at the CCSD(T)/CBS level with corrections for higher-order valence-electron correlation (using coupled cluster excitations up to CCSDTQP), core-valence correlation, scalar relativististic effects, and diagonal Born-Oppenheimer terms [12], with a subsequent very slight adjustment of two equilibrium geometry parameters against experimental data (changes in CH bond length by 0.0016 Å and in HCS angle by 0.02º) to improve the predicted intra-band rotational energy levels [81]. The dipole moment surface was computed at the CCSD(T)/aug-cc-pVQZ level (aug-cc-pv(Q+d)Z at sulfur) [81]. The rovibrational spectra calculated at T = 300 K are in excellent agreement with the available experimental data (see Figure 1). The TROVE calculations correctly reproduce the observed resonance effects (such as intensity borrowing), thus reflecting the high accuracy of the underlying ab initio surfaces. Experimentally, many high-resolution bands are still unassigned because of the complications arising from extremely strong Coriolis coupling (as pointed out by J. M. Flaud). Our detailed theoretical predictions and analysis of the rovibrational bands up to 5000 cm^{-1} (see e.g. Figures 2 and 3) are expected to facilitate and guide future laboratory assignments [81].

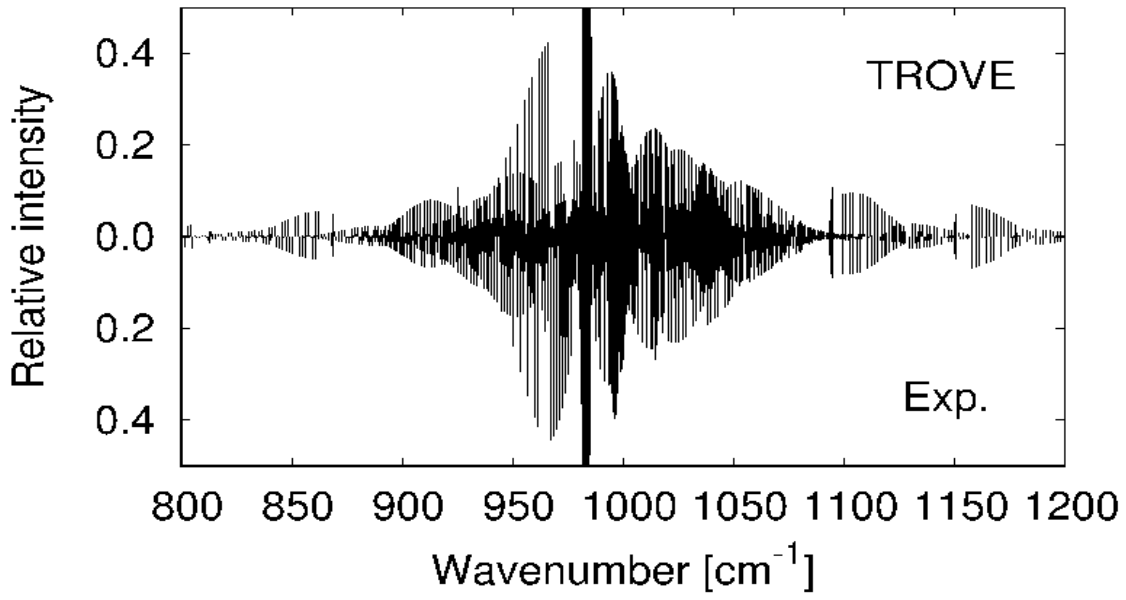

Figure 1. Comparison of the simulated absorption (T = 300 K) spectrum (TROVE) and the experimental spectrum (Exp.) of H_2CS for ν_4 and ν_6 bands [81].

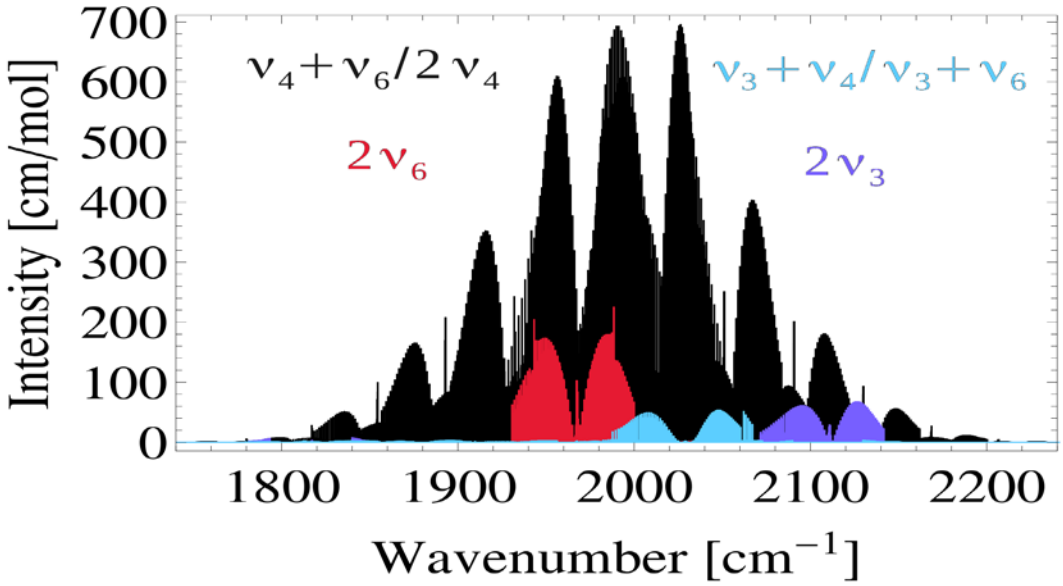

Figure 2. Overview of the simulated absorption spectrum of H_2CS at T = 300 K in the frequency range 1800-2200 cm^{-1} [81].

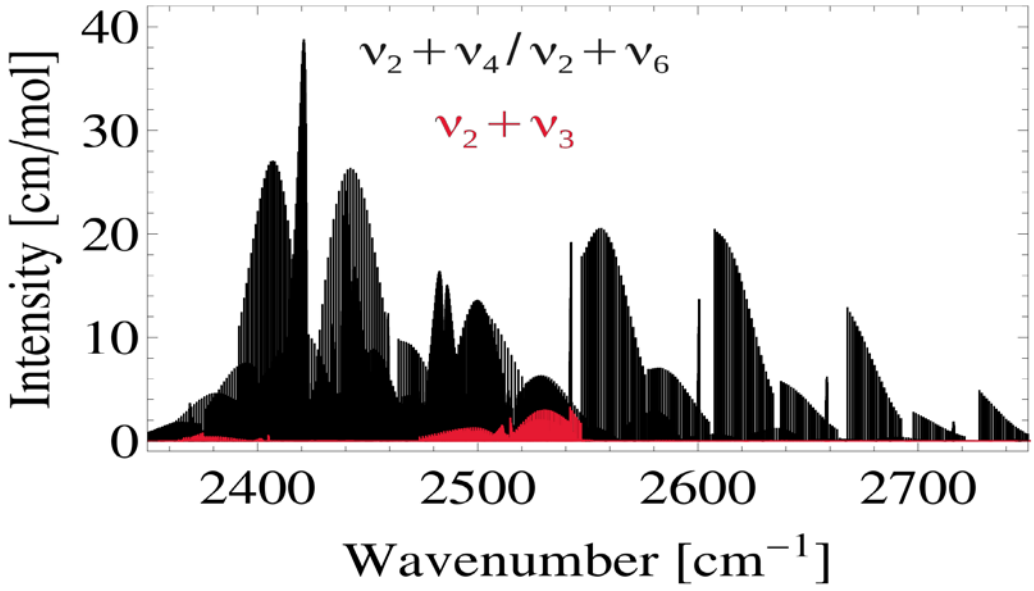

Figure 3. Overview of the simulated absorption spectrum of H_2CS at T = 300 K in the frequency range 2300-2800 cm^{-1} [81]. Please note different intensity scales in Figures 2-3.

In the case of formaldehyde H_2CO, we computed a CCSD(T)/aug-cc-pVQZ potential surface and refined it against spectroscopic data, achieving a root-mean-square (rms) deviation of 0.05 cm^{-1} for 599 rovibrational levels up to J = 5 [7]. In the case of ammonia, we refined our previously computed ab initio potential energy surface against accurate literature data covering transitions up to J = 8 and energy levels up to 10,300 cm^{-1} (with the constraint that the resulting surface remain close to the ab initio surface). This allowed us to reproduce the experimental term values of $^{14}NH_3$ with an rms

deviation of 0.05 cm^{-1} [15]. In collaborative work with the Marquardt and Quack groups, our ab initio surface was also used in the construction of an analytic, full-dimensional, and global representation of the potential energy surface of ammonia in the lowest adiabatic electronic state [71]. In the case of methane, we calculated a nine-dimensional dipole moment surface at the explicitly correlated CCSD(T)-F12c/aug-cc-pVTZ-F12 level and derived an accurate analytic representation using sixth-order polynomials, which will be used to produce comprehensive hot line lists for $^{12}CH_4$ (for astrophysical purposes such as modeling molecular opacity in the atmospheres of exoplanets and brown dwarfs) [76].

During the reporting period, we have published two reviews on ab initio rovibrational spectroscopy. The first one addresses the prediction of vibrational spectra from ab initio theory and the interplay between experiment and theory in the spectroscopic identification of new molecules, in particular reactive short-lived species [13]. The second one (together with T. J. Lee) reviews the use of quartic force fields in variational calculations of vibrational frequencies of small molecules, with emphasis on the choice of suitable coordinates with proper limiting behavior and on the accuracy that can be achieved in this manner [63].

Turning to electronically excited states and electronic spectroscopy, correlated ab initio calculations (e.g. at the MS-CASPT2 level) are performed for comparison or validation on a regular basis in excited-state projects that utilize lower-level methods (see the next chapters). In the reporting period, there have also been two ab initio application studies in this area. The first one concerned the electronically excited states and the photodissociation of benzaldehyde and acetophenone [31]. Our CASPT2//CASSCF calculations identify an $S_1/T_2/T_1$ three-state intersection area, where the T_2 state acts as a relay for an efficient $S_1 \rightarrow T_1$ intersystem crossing, followed by radical dissociation in the T_1 state. The computed pathways rationalize the experimental finding that different C-C bonds are cleaved in the photodissociation of benzaldehyde and acetophenone [31]. The second one addressed photoinduced gold(I)-gold(I) bonding in dicyanoaurate oligomers [74]. In collaboration with the Dolg and Fang groups, we assigned the band maxima of the oligomers $[Au(CN)_2^-]_n$ (n = 2-5) in aqueous solution on the basis of MS-CASPT2 calculations and explained the strengthening of the Au-Au bond upon excitation by considering the decisive orbital interactions in the leading configurations. The photodynamics in the oligomers could be well described by a three-state model for the staggered conformers and by a five-state model for the eclipsed conformers [74].

2.5.2 Research Area "Density Functional Methods" (W. Thiel)

Involved: A. Anoop, T. Benighaus, D. Escudero, G. Gopakumar, J. P. Götze, B. Heggen, C. Loerbroks, M. Patil, T. Saito, K. Sen, L. Wolf

Objective: Density functional methods are applied in studies of transition metal and other compounds in order to understand and predict their properties. Much of the work on homogeneous transition metal catalysis and organocatalysis involves a close collaboration with experimental groups at our Institute and aims at a detailed mechanistic understanding of the reactions studied experimentally. Methodological advances are targeted as required by the chosen projects.

Results: In many of our applications in this area, we employ state-of-the-art density functional theory (DFT) to explore the ground-state potential energy surface and to characterize all relevant intermediates, transition states, and reaction pathways. Geometry optimizations are normally done with standard functionals (RI-BP86, B3LYP, B3LYP-D) and medium-size basis sets, followed by higher-level single-point energy evaluations that utilize either correlated ab initio methods (e.g. local CCSD(T) treatments with large basis sets) or modern density functionals (e.g., from the M06 series) with large basis sets and dispersion corrections (if appropriate). Effective core potentials are normally used to represent the core electrons of heavy elements. Thermal and entropic corrections are computed at the level applied for geometry optimization.

Joint projects with the Fürstner group: Asymmetric gold catalysis with one-point binding ligands (phosphoramidites with TADDOL-related but acyclic backbone) enables a number of difficult transformations with excellent enantioselectivity. Our DFT calculations on the cycloisomerization of enynes helped elucidate the origin of the enantioselectivity achieved with such gold catalysts [42]. Gold carbenoids are commonly considered as intermediates in many Au-catalyzed reactions. Attempts to prepare germane gold carbenoids devoid of stabilizing substituents via transmetalation led to remarkable hetero-bimetallic complexes (e.g., containing Au and Cr) that were characterized at the DFT level in terms of their electronic structure and chemical bonding [84]. In the enantioselective gold-catalyzed intramolecular etherification of allenes, the preferred enantiomer has been found to depend on the choice of solvent as well as on the temperature. Through DFT-based modeling, we attempt to help rationalize this very unusual phenomenon, which may be due to different catalyst conformations being favored in different solvents (work by L. Wolf). Further unpublished work includes theoretical studies on iron catalysis (by B. Heggen).

Joint projects with the Alcarazo group: The research in the Alcarazo group is directed towards the design and synthesis of unusual ligands and coordination compounds and their application in novel catalytic transformations. In our collaborative work, we perform DFT calculations to characterize the electronic structure of key species and to unravel the detailed mechanism of the catalytic reactions. Examples include the analysis of the electronic structure in the first observed dihydrido borenium cation [16], in carbene-stabilized phosphorus(III)-centered trications [22], in carbene-stabilized N-centered cations [54], and in cationic Ge(II) complexes [60]. In the latter case, the stability of the complexes arises from the ability of the neutral monodentate hexaphenylcarbodiphosphorane ligand to donate two electron pairs and thus simultaneously form two dative C = Ge σ and π bonds [60]. The pronounced π-acceptor properties of phosphorous trications [22] can be exploited in Pt(II) catalysis [44] and in gold catalysis [83] to enable very demanding cyclization reactions. We elucidated the underlying reaction mechanisms by computing the free energy profiles for the cyclization of 2-ethynyl-1,1'-binaphthalene into pentahelicene [44] (see Figure 4 as a typical example of such work) and of 2-ethynyl-2',6-dimethylbiphenyl into 4,5-dimethylphenanthrene [83].

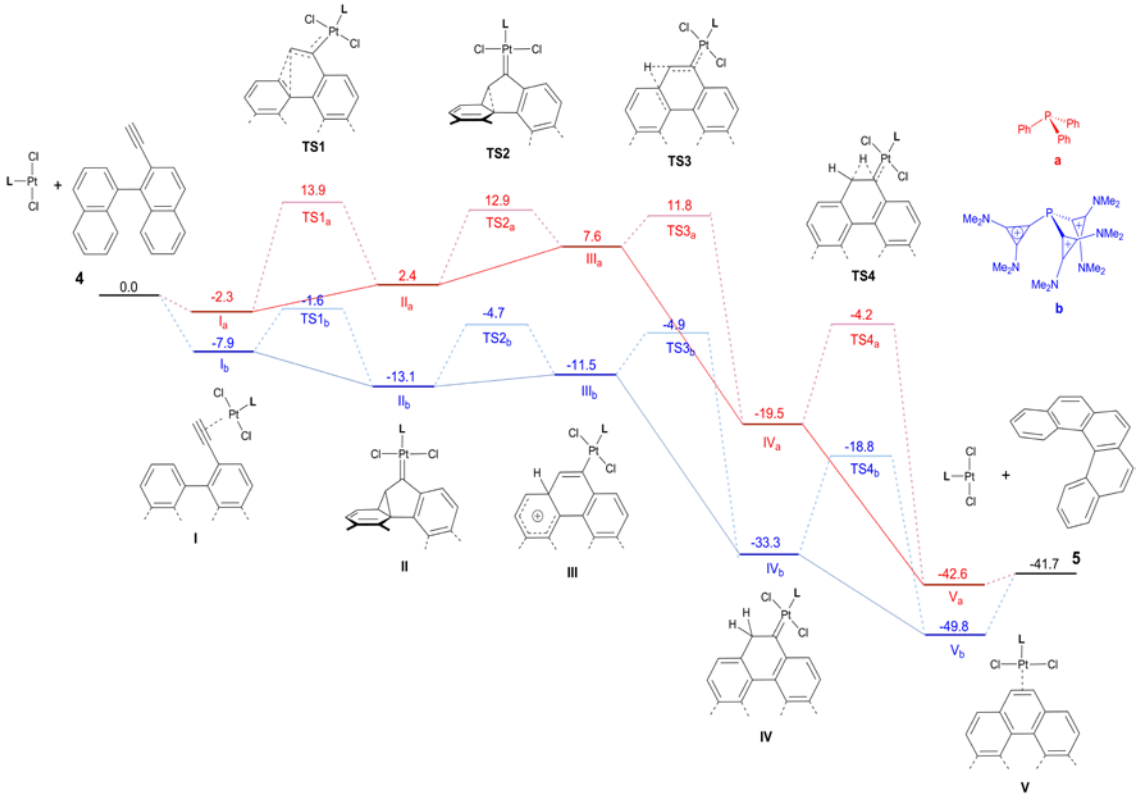

Figure 4. Free energy profiles (kcal/mol) for the cyclization of 2-ethynyl-1,1'-binaphthalene into pentahelicene, computed at the B3LYP-D level with a large basis set and PCM corrections [44]. Red: L = Ph_3P; blue: L = phosphorus trication $[R_3P]^{3+}$ with R = 2,3-dimethylamino-cyclopropenyl-1-ylidene. Calculated LUMO energies [44] for ligands L: -3.28 eV (red) vs. -11.69 eV (blue).

Joint projects with the List group: Chiral phosphoric acids are able to catalyze asymmetric S_N2-type O-alkylations, which formally involve a nucleophilic attack at the σ* orbital of a carbon electrophile. DFT calculations on the mechanism of a representative TRIP-catalyzed intramolecular alkylation show that the Brønsted acid acts as a bifunctional activator bridging the pentacoordinate transition state [52]. High stereoselectivity can be achieved in the asymmetric epoxidation and hydroperoxidation of α,ß-unsaturated carbonyl compounds using alkaloid-derived primary amines as catalysts and aqueous hydrogen peroxide as oxidant. Here, the analysis of the computed pathways led to a qualitative model of enantioselectivity based on the structure of the crucial iminium intermediate [58]. Still unpublished are further DFT investigations on the nature of the transition state in the catalytic 6π electrocyclization of unsaturated hydrazones.

Joint projects with the Maulide group: Sulfur (IV)-mediated transformations can be used to achieve direct ylide transfer to and metal-free arylation of carbonyl compounds, depending on the reagent (Martin's sulfurane or activated sulfoxides). Mechanistic studies (via NMR and DFT) support a common reaction pathway via very similar cationic S(IV) species and showcase how subtle changes in reactant properties can lead to disparate and seemingly unrelated reaction outcomes [61]. On a different front, the Maulide group has recently discovered the phenomenon of catalytic asymmetric diastereodivergent deracemization in Pd-catalyzed allylic alkylations. As part of a follow-up study, we performed DFT calculations that provide detailed insight into the Pd-catalyzed electrocyclic ring opening of cyclobutene units in large molecules, which proceeds as a conrotatory reaction in an intermediate Pd-cyclobutene complex, with competing isomer interconversion by η^1-η^3-η^1 allyl slippage [64]. Further DFT results are available on the detailed mechanism of other steps in the ligand-controlled deracemization (unpublished work by G. Gopakumar and L. Wolf).

Joint projects with the Rinaldi and Schüth groups: Cellulose consists of 1,4-β-linked glucose units, which can be converted to biofuel and industrial platform molecules. The depolymerisation of cellulose to glucose is an important part of this conversion process. As a first step in modeling this process, we have explored the electronic nature of the 1,4-β-glycosidic bond and its chemical environment in cellobiose (glucose dimer) as well as its influence on the mechanism of the acid-catalyzed hydrolysis [78]. The DFT results imply that cellulose is protected against hydrolysis not only by its supramolecular structure (as commonly accepted), but also by its electronic structure, in which the anomeric effect plays a key role [78]. Ongoing follow-up work addresses the

depolymerization of larger cellulose models (up to 40 linked glucose units) in water and in ionic liquids using QM/MM calculations on the hydrolysis mechanism as well as classical metadynamics simulations on the influence of conformational changes. In a related project, the isomerization of glucose to fructose in water has been studied at the DFT level to clarify the detailed reaction mechanism and to rationalize the observed differences in the catalytic efficiency of different metal cations (unpublished work by C. Loerbroks).

Other ground-state DFT projects: Some mechanistic DFT studies have been carried out without involvement of experimental groups from the Institute. These include calculations on the origin of selectivity in Pd-catalyzed Tsuji-Trost allylic alkylation reactions [18, 37] and on the mechanism of the stereoselective Pummerer reaction [56]. In the context of collaborative spectroscopic work with the Havenith and Sander groups (Bochum), we have performed DFT-based molecular dynamics (MD) simulations on acetylene-furan trimer formation in ultracold helium droplets to follow the aggregation process towards the global minimum [9] and on complexes between aromatic radicals and water to assess their stability at different temperatures and the population of different local minima [53].

Excited-state DFT projects: In our semiempirical excited-state work, DFT-based calculations are often carried out for comparison or validation (see the next chapter). In addition, there have been three application studies in the reporting period that mainly rely on time-dependent density functional theory (TD-DFT). In collaboration with the Barbatti group, we performed TD-DFT benchmark calculations on donor-acceptor heterojunctions composed of thiophene oligomers and C_{60} fullerene to identify the most suitable functional for studying organic solar cells of this kind [49]. The electronic excitations of two carotenoids (violaxanthine and zeaxanthine) were computed in the gas phase and in acetone using different DFT-based approaches to assess their performance, which turned out to be most favorable for the Coulomb attenuated CAM-B3LYP functional [55]. In cooperation with the Holder group, we investigated the photodeactivation pathways in a novel Ir(III) cyclometalated complex, a promising candidate for electroluminescent devices. Our DFT and TD-DFT calculations indicate that metal-centered triplet excited states play an active role in the nonradiative deactivation of this complex [77].

Analytic gradients: Unrestricted density functional theory (UDFT) is widely applied to open-shell systems. UDFT treatments often yield broken-symmetry (BS) spin-polarized

solutions that capture a certain amount of nondynamical correlation but suffer from spin contamination, which may be removed by spin projection schemes to obtain improved single-point energies. We have derived and implemented analytic gradients for BS-UDFT calculations with removal of spin contamination by Yamaguchi's approximate spin projection method [45]. The analytic gradients are more precise, robust, and efficient than the previously available numerical gradients, and they allow fast full geometry optimizations of large open-shell systems, as shown in several test applications [45].

Stochastic simulations: Motivated by experimental work in the Reetz group showing that rhodium catalysts with chiral monodentate phosphorous ligands can achieve asymmetric hydrogenation with high efficiency and enantioselectivity, we had previously computed at the DFT level the entire catalytic cycle for enantioselective hydrogenation of itaconic acid using a chiral Rh(phosponite)$_2$ catalyst. In the present reporting period, the computed relative free energies of all stationary points in the four coupled lowest-energy cycles leading to (*R*)- and (*S*)-product were refined by single-point calculations using accurate domain-based local pair natural orbital coupled cluster theory (DLPNO-CCSD and DLPNO-CCSD(T), unpublished work with the Neese group). To analyze the chemical kinetics of this reaction (with 20 stationary points in each of the four coupled cycles), we have implemented Gillespie's stochastic simulation algorithm (SSA) including various options such as τ leaping in the code. Kinetic Monte Carlo simulations with the SSA algorithm were performed to determine the enantiomeric excess (*ee*) in the products for several temperatures and for several sets of computed relative energies. The resulting *ee* values were found to be very sensitive to the input energies, and large differences were encountered for different DFT approaches. Good agreement with experiment was obtained at the coupled cluster level (unpublished work by J. Breidung).

2.5.3 Research Area "Semiempirical Methods" (W. Thiel)

Involved: G. Cui, P. Dral, E. Fabiano, J. A. Gámez, B. Heggen, M. Korth, A. Koslowski, Z. Lan, Y. Lu, A. Nikiforov, L. Spörkel, O. Weingart, X. Wu

Objective: This long-term project aims at the development of improved semiempirical quantum-chemical methods that can be employed to study ever larger molecules with useful accuracy. This includes the development of more efficient algorithms and computer programs. Our current focus in this area is on electronically excited states.

Results: Over the past years, we have developed semiempirical methods that go beyond the standard MNDO model by including orthogonalization corrections at the NDDO level. This has led to three new approaches labelled OM1, OM2 and OM3 (orthogonalization models 1-3) that offer significant improvements over established MNDO-type methods in several areas, including conformational properties, hydrogen bonds, reaction barriers, and electronically excited states.

During the reporting period, we have rewritten our code for the multi-reference configuration interaction (MR-CI) treatment of electronically excited states. We have replaced the loop-driven by a shape-driven version of the GUGA-CI algorithm (GUGA, graphical unital group approach). We have implemented an in-core and a direct variant of the algorithm, in which the CI coupling coefficients are stored explicitly or recomputed as needed, respectively. The new code is about twice as fast as the old one (unpublished work by A. Koslowski).

In the self-consistent-field (SCF) part of our semiempirical MNDO code, we have implemented two algorithms that allow for non-integer occupation numbers of the orbitals. *Fermi smearing* introduces some occupation of virtual orbitals at high electronic temperatures and improves SCF convergence. OM2 with Fermi smearing has recently been recommended for the simulation of electron impact mass spectra of organic molecules (S. Grimme, Angew. Chem. Int. Ed. 2013, 52, 6306). The *floating occupation number SCF treatment* aims at improving the shape of the relevant active orbitals such that they are well suited for MRCI calculations on excited states. Analytic gradients have been implemented for this approach.

On the technical side, the SCF section of our semiempirical MNDO code has been ported to hybrid CPU-GPU platforms that contain a graphics processing unit (GPU) as a

co-processor [33]. The most time-consuming routines were optimized for GPUs by using suitable library routines for linear algebra tasks and locally written GPU kernels for pseudodiagonalization and for orthogonalization corrections. The overall computation times for single-point energy calculations and geometry optimizations of large molecules were reduced typically by one order of magnitude for all semiempirical methods, as compared to runs on a single CPU core [33]. This development makes it practical to study whole proteins at the semiempirical SCF level. In addition, the in-core variant of the Davidson-Liu diagonalizer was also ported to GPUs to speed up large-scale MRCI calculations (unpublished work by A. Koslowski).

For validation purposes, the accuracy of six standard semiempirical methods has been benchmarked [17] using the comprehensive GMTKN24 database for general main group thermochemistry, kinetics, and noncovalent interactions, which had originally been introduced to evaluate DFT methods (L. Goerigk and S. Grimme, J. Chem. Theory Comput. 2010, 6, 107). The OMx methods outperform AM1, PM6, and SCC-DFTB by a significant margin, with a substantial gain in accuracy especially for OM2 and OM3. These latter methods are quite accurate and robust even in comparison to DFT, with overall mean absolute deviations in the computed energies of 6.6 kcal/mol for PBE and 7.9 kcal/mol for OM3 [17].

In cases where the generic accuracy of semiempirical methods is not sufficient for a given application, it is possible to perform specific parameterizations. During the reporting period, this has been done in two collaborative projects: In the first one (with D. T. Major), specific reaction parameters (SRP) were derived in the AM1 framework for dihydrofolate reductase (DHFR) to enable accurate quantum mechanics/molecular mechanics (QM/MM) molecular dynamics (MD) simulations of the DHFR-catalyzed reaction and the evaluation of reliable kinetic isotope effects using a mass-perturbation-based path-integral approach [20]. The second project (with H. Lin) involved the reparameterization of the AM1, PM3, and OMx methods to improve their description of bulk water and of proton transfer in water. QM/MM MD simulations with the resulting SRP Hamiltonians led to significantly better results in all cases, with OM3 accounting best for the structural and dynamic properties of water and the hydrated proton [66].

Over the past three years, our semiempirical applications have focused on excited-state dynamics. We had previously implemented the trajectory surface hopping (TSH) method with the fewest switches algorithm (Tully) in the MNDO software, making use of our semiempirical in-core version of the GUGACI method that handles general CI

expansions (up to full CI) efficiently for small active spaces and provides an analytic GUGACI gradient as well as analytic nonadiabatic coupling matrix elements. Most of these studies were carried out at the OM2/MRCI level for medium-size organic molecules in the gas phase. These TSH simulations provided insight into the chiral pathways and mode-specific tuning of photoisomerization in azobenzenes [6,34,67], the mechanism of hexatriene-based fulgide photoswitches [40] and Feringa-type fluorene-based photoinduced molecular rotors [10], the complete photochemical cycle of a GFP chromophore with ultrafast excited-state proton transfer [24], the preferred relaxation pathways in the nonadiabatic dynamics in 4-N,N-dimethylamino-benzylidene malononitrile (a typical push-pull charge transfer system) [28], the photophysics of a truncated indogo model [41], the competition between concerted and stepwise mechanisms in the ultrafast photoinduced Wolff rearrangement of 2-diaza-1-naphthoquinone [48] (see Figure 5), and the photodynamics and photochromism in the prototypical Schiff base salicylidenaniline [65]. The results of these OM2/MRCI studies are generally consistent with the available experimental data and high-level static calculations, but the dynamics simulations often detect pathways and preferences between pathways that are not obvious from the static calculations. The OM2/MRCI approach has thus emerged as a suitable tool for investigating the excited states and the photochemistry of large molecules.

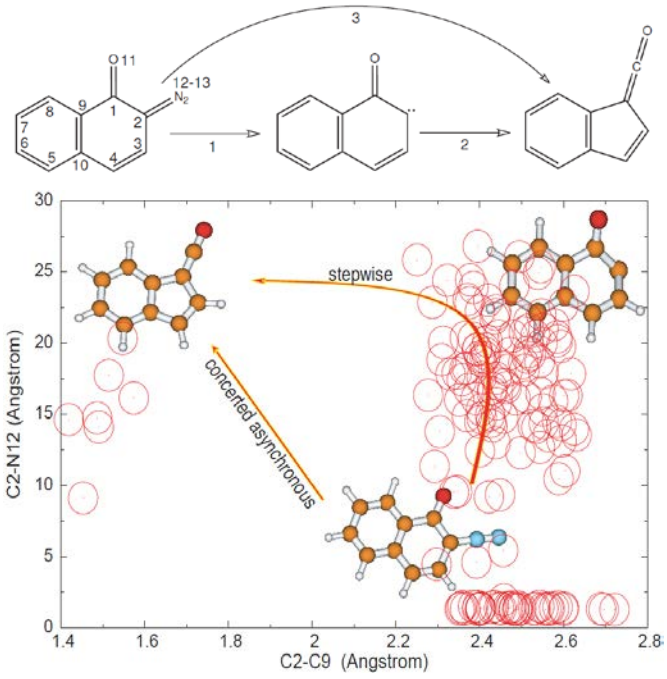

Figure 5. Top: Wolff rearrangement of 2-diazo-1-naphthoquinone (DNQ): stepwise (1-2) and concerted (3) mechanisms; the numbering scheme for the atoms is shown for the DNQ reactant. Bottom: Product distribution among 158 trajectories at the end of the 1 ps nonadiabatic simulations; red circles indicate the final geometries [48].

Note concerning Figure 5: The ketene product of the concerted Wolff rearrangement is found in 7 out of 158 trajectories; 39 trajectories return to the ground-state starting point, and the remaining 112 trajectories are roaming the carbene region. In subsequent 10 ps Born-Oppenheimer molecular dynamics for the carbene, using the final positions and velocities of the carbene fragment in the TSH trajectories as initial conditions, 36 of the 112 trajectories evolve from the "hot" carbene to the ketene region, thus increasing the overall ketene quantum yield to ca. 27% after 10 ps [48].

In the previous reporting period, we had already studied the excited-state dynamics and the photostability of the nucleobases in the gas phase. In joint work with M. Barbatti, we have thereafter carried out a thorough benchmark on *9H*-adenine [35] comparing the TSH results from ab initio MR-CIS, TD-DFT, and OM2/MRCI gas-phase simulations. The ab initio and OM2/MRCI methods predict the experimentally observed ultrafast deactivation of *9H*-adenine with similar time scales (but through different internal conversion channels), whereas the TD-DFT calculations with six different hybrid and range-corrected functionals fail to predict the ultrafast deactivation. These discrepancies were traced back to the topographies of the underlying potential energy surfaces along the relevant reaction pathways [35].

Using our TSH implementation in the ChemShell QM/MM framework, we have also studied the nonadiabatic dynamics of nucleobases in aqueous solution (adenine, guanine) and in model DNA strands (adenine). Going from the gas phase to aqueous solution, the optimized geometries of the relevant conical conical intersections and the associated relaxation paths remain qualitatively similar, but there are changes in their relative importance because of the solvent-induced shifts in the energetics. Overall, the decay times in solution are even slightly lower than those in the gas phase [8,32]. By contrast, the S_1 lifetime of adenine in a solvated B-type DNA oligomer model $(dA)_{10}$ is computed to be about ten times larger (ca. 5 ps) than in the gas phase. This is at least partly due to the higher rigidity of the DNA strand, since the two relevant conical interactions are both characterized by strong out-of-plane deformations that are more difficult to reach in the DNA environment. In our DNA double strand model, solvated $(dA)_{10}{\cdot}(dT)_{10}$, one of these two decay paths is suppressed because the out-of-plane motion of the amino group is impeded by inter-strand hydrogen bonding [11,30].

Ground-state MD simulations of large systems can be computationally demanding even at the QM/MM level and often become practical only with semiempirical QM methods. We use such semiempirical QM/MM MD simulations regularly in QM/MM projects [2,20,26,27,66,68,70], for example in free energy calculations or to follow the time evolution of complex systems. This work will be described in the next section.

2.5.4 Research area "Combined Quantum Mechanical / Molecular Mechanical Methods" (W. Thiel)

Involved: A. Altun, T. Benighaus, E. Boulanger, M. Doerr, E. Fabiano, J. P. Götze, B. Heggen, Y. Hsiao, B. Karasulu, Z. Lan, R.-Z. Liao, Y. Lu, S. Metz, M. Patil, I. Polyak, E. Sánchez-García, K. Sen, M. R. Silva-Junior, T. Vasilevskaya, O. Weingart, X. Wu

Objective: This research focuses on hybrid approaches for large systems where the active center is treated by an appropriate quantum mechanical method and the environment by a classical force field. It involves considerable method and code development. This approach allows a specific modeling of complex systems such that most of the computational effort is spent on the chemically important part. Current applications primarily address biocatalysis and aim at a better understanding of enzymatic reactions including the role of the protein environment.

Results: Combined quantum mechanical/molecular mechanical (QM/MM) methods have become a popular tool for studying reactions in complex systems such as enzymes. In the preceding reporting period, we had extended the two-layer QM/MM approach to a three-layer model by introducing boundary potentials that represent the outer part of the MM region and the bulk solvent. This offers two major advantages: conceptually, the long-range electrostatic interactions in a solvated enzyme are well described in this manner, and technically, the computational effort is reduced significantly by the strong reduction of the number of explicitly treated MM atoms (typically 2,000 compared with around 30,000 in standard QM/MM work). We previously implemented the generalized solvent boundary potential (GSBP), known from MM-MD simulations, in a semiempirical QM/MM framework (JCTC 2008, 4, 1600). In a second step, we developed a new boundary potential (SMBP, solvated macromolecule boundary potential) that is conceptually similar to GSBP, but can be used with any QM method and is also efficient for geometry optimization (JCTC 2009, 5, 3114). We have applied these boundary potential techniques to study the influence of long-range electrostatic interactions on the enzymatic reactions in chorismate mutase (CM) and p-hydroxybenzoate hydroxylase (PHBH) [2]. The corresponding energetic effects were found to be small for the pericyclic Claisen rearrangement catalyzed by CM (with little charge transfer), but substantial (several kcal/mol) for the hydroxylation reaction in PHBH, during which there is a formal transfer of one negative charge from the substrate to the cofactor. The QM/MM/SMBP approach provides detailed insight into the electrostatic influence of the outer MM region and the bulk solvent [2].

Our first three-layer QM/MM/continuum treatments combined the polarizable QM region with a fixed-charge MM region and a bulk solvent represented by a polarizable dielectric continuum (PDC). To arrive at a fully polarizable three-layer model, polarizable MM force fields were implemented in our QM/MM/BP approach [46] using the classical Drude oscillator (DO) model for the electronic polarizability of the MM atoms. As the mutual responses of each subsystem must be taken into account, efficient schemes were developed to converge the polarization of each layer simultaneously. This was achieved by considering the MM polarizable model as a dynamical degree of freedom in MD simulations with GSBP, and by using a dual self-consistent-field procedure for relaxing the Drude oscillators to their ideal positions and for converging the QM wavefunction in geometry optimizations with SMBP [46]. Applications with this new fully polarizable three-layer treatment are currently in progress.

The proper initial system setup for QM/MM studies is non-trivial. Starting geometries are commonly taken from classical MD simulations, but random MD snapshots may contain regions with high-energy conformations. In cooperation with the Engels group, we have proposed a new approach for the setup of water shells around proteins employing Tabu-Search global optimization techniques [50]. Comparisons with standard MD protocols for the chignolin test case show that both algorithms are capable of providing reasonable water shells. The new approach offers the advantage to generate more stable solvated systems with increased water-enzyme interactions and to enable a stepwise build-up of the solvent shell, such that the more important inner part can be prepared more carefully [50].

In QM studies of small molecules, transition states are normally verified by following the intrinsic reaction coordinate (IRC) towards reactants and products. Such IRC computations are difficult at the QM/MM level because of the high dimensionality of the investigated systems. To overcome these problems, we adopted a strategy analogous to microiterative transition state optimization. In this approach [69], the IRC equations only govern the motion of a core region that contains at least the atoms directly involved in the reaction, while the remaining degrees of freedom are relaxed after each IRC step. This strategy can be used together with any existing IRC procedure. After some proof-of-principle tests at the QM level on small gas-phase systems, the broad applicability of our implementation was demonstrated by IRC computations for two real-life enzymatic reactions using standard QM/MM setups [69].

Free energy calculations are demanding at the QM/MM level because of the need for extensive sampling. They are technically feasible with semiempirical QM components, and there are several approximate treatments available in combination with high-level

QM treatments. We designed a dual Hamiltonian free energy perturbation (DH-FEP) method for accurate and efficient evaluation of the free energy profile of chemical reactions in QM/MM calculations [70]. In contrast to existing QM/MM FEP variants, the QM region is not kept frozen during sampling, but all degrees of freedom except for the reaction coordinate are sampled. In the DH-FEP scheme, the sampling is done by semiempirical QM/MM MD simulations, while the perturbation energy differences are evaluated from high-level QM/MM single-point calculations at regular intervals, skipping a pre-defined number of MD sampling steps. The merits of the QM/MM DH-FEP approach were demonstrated by free energy calculations for an analytic model potential with an exactly known solution (validation) and for the enzymatic reaction catalyzed by CM. In the latter case, the DH-FEP approach was applied in combination with a one-dimensional reaction coordinate and with a two-dimensional collective coordinate (two individual distances), with superior results for the latter choice [70].

For the modeling of enzymatic reactions, QM-only calculations on model systems may be used as an alternative to QM/MM calculations on the full solvated enzyme. We compared these two approaches in a case study [43,75] on the formation of vinyl alcohol in the catalytic cycle of tungsten-dependent acetylene hydratase (AH). Seven QM regions were considered, containing 32 up to 657 atoms, which were selected on the basis of charge deletion analysis and distance criteria. Overall, the QM/MM energies were found to converge more smoothly than the QM-only energies upon increasing the size of QM region. At the QM/MM level, the reaction mechanism is qualitatively well described when using 157 QM atoms, whereas quantitative convergence in the computed relative energies to within 1-2 kcal/mol requires a large QM region with 407 atoms in the case of AH [43,75]. Another issue in QM-only studies of enzymatic reactions (apart from convergence with regard to model size) is the use of a coordinate-locking scheme, in which certain key atoms at the periphery of the chosen cluster model are fixed to their crystal structure positions. In a further case study on AH [57], we investigated the uncertainties introduced by this scheme, which arise from the limited accuracy of the experimental crystal structures. We found that the resulting uncertainties in the QM-only energies are tolerable for high-quality protein crystal structures (resolution better than 2.0 Å), but may become unacceptable for structures with significantly lower resolution [57].

In the preceding reporting period, we had implemented quantum refinement into our ChemShell QM/MM software. The traditional procedure for solving protein crystal structures is to supplement the X-ray diffraction data with restraints from simple MM force fields during the refinement. These restraints are taken from QM/MM energies in quantum refinement, which should thus be more reliable especially in regions that are

not well described by the available MM force fields. We applied quantum refinement in combination with classical MD simulations, QM/MM geometry optimizations, and DFT/MRCI calculations of electronic absorption spectra to reinvestigate the structure of the pB_2 species in the photocycle of the photoactive yellow protein [3] and of the blue-light sensing using flavin (BLUF) domain of the wild-type AppA protein from *Rhodobacter sphaeroides* [36]. In the pB_2 case, this led to an improvement of the chromophore geometry towards a somewhat more planar structure and the identification of a previously overlooked crystal water molecule near the phenolic OH group of the chromophore [3]. In the AppA BLUF case, there are two published crystal structures (1YRX and 2IYG) that give different side-chain orientations of key residues close to the flavin chromophore (e.g., Gln63) – our calculations slightly favor the 1YRX-type orientation [26,36].

In QM/MM studies on enzymatic reaction mechanisms, we normally use geometry optimization techniques to follow conceivable pathways on DFT/CHARMM potential energy surfaces in order to determine the most favorable one. Optimizations are normally done with efficient DFT approaches (e.g., RI-BP86 with moderate basis sets), while relative energies are determined using more refined functionals (e.g., B3LYP-D or M06 with larger basis sets) or even correlated ab initio methods (CCSD(T) or multi-reference treatments). If necessary, QM/MM free energy calculations are performed to capture entropic contributions. In the following, we first describe one such mechanistic QM/MM study in some detail and then briefly summarize several others.

Motivated by experimental directed evalution work in the Reetz group, we examined the Baeyer-Villiger oxidation reaction in cyclohexanone monooxygenase (CHMO) to elucidate its mechanism and the origin of its enantioselectivity. According to the QM/MM calculations on the wild-type enzyme [27], the enzyme-reactant complex contains an anionic deprotonated C4a-peroxyflavin that is stabilized by strong hydrogen bonds with the ARG-329 residue and the $NADP^+$ cofactor. The CHMO-catalyzed reaction proceeds via a Criegee intermediate with pronounced anionic character. The fragmentation of this intermediate to the lactone product is the rate-limiting step. The QM/MM results for the parent cyclohexanone confirm the crucial role of the ARG-329 residue and of the $NADP^+$ cofactor for the catalytic efficiency of CHMO. QM/MM calculations for the CHMO-catalyzed oxidation of 4-methylcyclohexanone reproduce and rationalize the experimentally observed (*S*)-enantioselectivity for this substrate, which is governed by the conformational preferences of the corresponding Criegee intermediate and the subsequent transition state (TS2) for the migration step [27]. A subsequent QM/MM study addressed the effect of mutations of the Phe434 residue in the active site of CHMO on its enantioselectivity towards 4-hydroxycyclohexanone

[59]. In terms of our previously established model of the wild-type enzymatic Baeyer-Villiger reaction, enantioselectivity is governed by the preference towards the equatorial ((*S*)-selectivity) or axial ((*R*)-selectivity) conformation of the substituent at the C4 carbon atom of the cyclohexanone ring in the Criegee intermediate and the rate-limiting transition state (TS2). The enantiopreference towards 4-hydroxycyclohexanone was assessed by locating all relevant TS2 structures at the QM/MM level, for the wild-type enzyme and two mutants (Phe434Ser and Phe434Ile). The experimentally observed enantioselectivity was reproduced semi-quantitatively in all three cases, including the pronounced reversed enantioselectivity in the Phe434Ser mutant. The effect of point mutations on CHMO enantioselectivity could be explained at the molecular level, by an analysis of the specific interactions between substrate and active-site environment in the TS2 structures (see Figure 6) that satisfy the basic stereoelectronic requirement of anti-periplanarity for the migrating σ-bond [59].

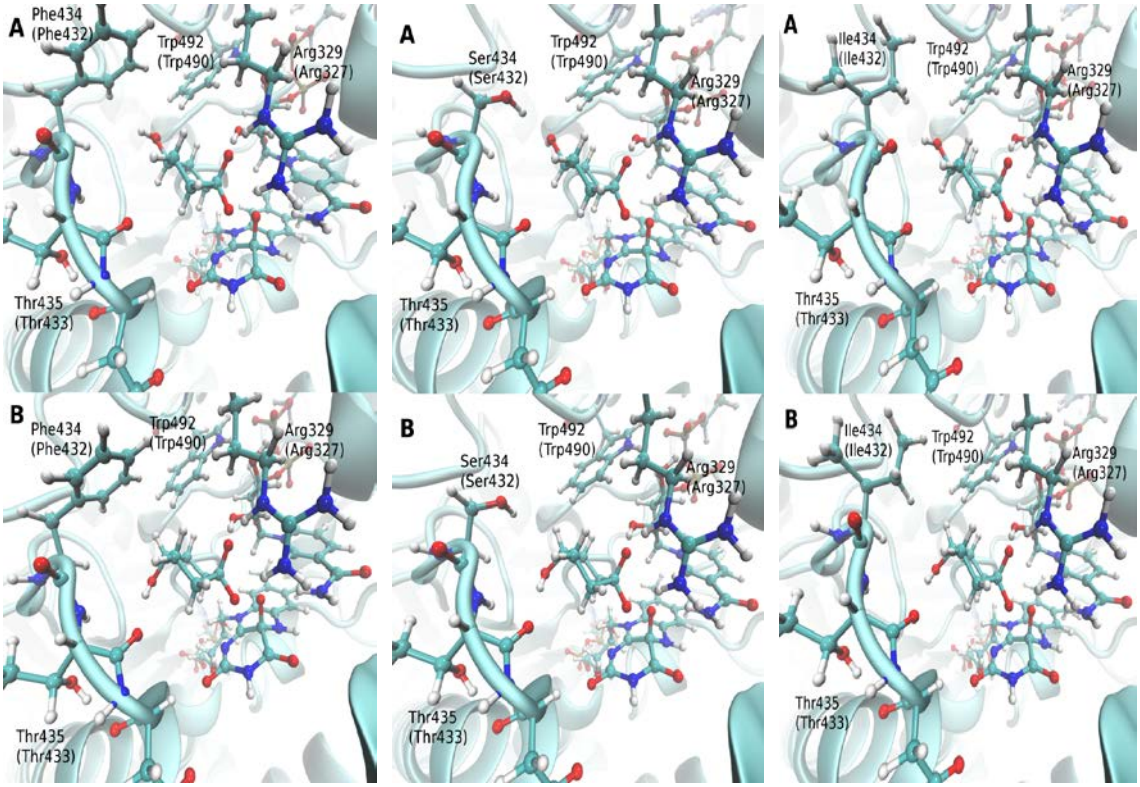

Figure 6. QM/MM optimized structures of the rate-limiting transition state for migration. Left: wild-type CHMO; middle: Phe434Ser mutant; right: Phe434Ile mutant. A (top): equatorial orientation of the substrate hydroxyl group. B (bottom): axial orientation of the substrate hydroxyl group.

Note concerning Figure 6: In orientation B, the substrate OH group always forms an H-bond with the Thr435 carbonyl oxygen atom. In orientation A, the substrate OH group interacts with the Phe434 phenyl ring of the wild-type CHMO (left), with the Ser434 OH group of the Phe434Ser mutant (middle), and with the isoleucine backbone carbonyl atom in the Phe434Ile mutant (right). The relative strength of these interactions determines the favored orientation, and hence the stereochemical outcome of the reaction. The equatorial orientation A is preferred only in the Phe434Ser mutant because of the strong H-bond between the OH groups of the substrate 4-hydroxycyclohexanone and the serine residue. Therefore, (*S*)-selectivity is only observed in the Phe434Ser mutant.

In the following, we briefly summarize the results from five other QM/MM studies on ground-state enzymatic reactions that were carried out during the reporting period.

(a) Glycosyltransferases (GTs) catalyze the highly specific biosynthesis of glycosidic bonds. We investigated the mechanism of the reaction catalyzed by Lipopolysaccharyl-α-1,4-galactosyltransferase C (LgtC) from *Neisseria meningitides* [29]. Among the three alternatives discussed in the literature, the QM/MM calculations favor a dissociative single-displacement (S_Ni) mechanism, in which the acceptor substrate attacks on the side of the UDP leaving group that acts as a catalytic base. They identify several key interactions that help this front-side attack by stabilizing the oxocarbenium ion-like transition state [29].

(b) Lysine-Specific Demethylase 1 (LSD1) catalyzes the demethylation of particular lysine residues in histone protein tails (H3K4), with flavin adenine dinucleotide (FAD) acting as cofactor. The oxidation of substrate lysine (sLys) involves the cleavage of an α-CH bond accompanied by the transfer of a hydride ion equivalent to FAD, leading to an imine intermediate. The QM/MM calculations predict this hydride transfer pathway to be clearly favored for sLys oxidation over other proposed mechanisms, including the single-electron transfer route or carbanion and polar-nucleophilic mechanisms [73]. They rationalize the activation of the rather inert methyl-CH bond in a metal-free environment through proper alignment of sLys and transition state stabilization, as well as the role of important active-site residues (Y761, K661, and W695) and of the conserved water-bridge motif [73].

(c) Fosfomycin A is a manganese-dependent enzyme that utilizes a Mn^{2+} ion to catalyze the inactivation of the fosfomycin antibiotic by glutathione (GSH) addition. According to our QM/MM calculations [51], the enzyme-catalyzed glutathione addition reaction proceeds in the sextet state. It involves an initial proton transfer from the GSH thiol group to the Tyr39 anion, followed by a nucleophilic attack of the GSH thiolate leading to epoxide ring opening. The second step is rate-limiting and is facilitated by the presence of the high-spin Mn^{2+} ion that functions as a Lewis acid and stabilizes the leaving oxyanion through direct coordination. The QM/MM calculations rationalize the observed catalytic efficiency, regioselectivity, and chemoselectivity of Fosfomycin A in terms of the influence of the active-site protein environment and the different stabilization of the distorted substrate in the relevant transition states [51].

(d) Aldoxime dehydratase is a heme-containing enzyme that utilizes the ferrous rather than the ferric ion to catalyze the synthesis of nitriles by dehydration of the substrate. Our QM/MM study of the enzymatic dehydration of *Z*-acetaldoxime covered all three

possible spin states [38]. Only one pathway was found to be feasible, starting with substrate coordination to Fe^{2+} via its nitrogen atom followed by N-O cleavage that is facilitated by a single-electron transfer from the ferrous heme to an antibonding N-O orbital in the singlet state, while His320 acts as a general acid and base by mediating the required proton transfers [38]. This scenario explains the observed oxidation state preference (Fe^{2+} vs. Fe^{3+}).

(e) Cysteine dioxygenase (CDO) is involved in the biodegradation of toxic cystein. It is a nonheme iron dioxygenase that transfers the two oxygen atoms from molecular oxygen to cysteinate to form cysteine sulfinic acid products. The mechanism for this reaction is disputed in the literature. Our QM/MM calculations [4] on substrate activation by CDO give a stepwise mechanism that takes place on several low-lying spin state surfaces via multistate reactivity patterns, starting on the singlet ground state of the iron(II)-superoxo reactant and then proceeding mainly on the quintet and triplet surfaces. An alternative pathway via a persulfenate intermediate is much higher in energy and thus not accessible [4].

In the area of ground-state enzyme reactivity, we have also published reviews on our previous QM/MM studies of molybdenum-containing enzymes [5] and on the role of single water molecules as biocatalysts in cytochrome P450cam chemistry [1]. Still unpublished is mechanistic QM/MM work on the P450eryF enzyme (by K. Sen) and on hemocyanin (by T. Saito).

Turning to QM/MM applications on electronically excited states, we have already mentioned in the preceding chapter the semiempirical QM(OM2/MRCI)/MM surface hopping studies of nucleobases in water and in DNA strands [8,11,30,32]. We have also performed QM/MM calculations of electronic absorption spectra in the condensed phase, most notably on rhodopsin mutants linked to the *Retinitis pigmentosa* disease [25], the red fluorescent protein (HcRed) from *Heteractis crisp* [39], and the blue-light photoreceptor YtvA of *Bacillus subtilis* with structurally modified flavin chromophores [72]. The QM/MM calculations of the electronic spectra mostly employed DFT/MRCI as QM component. In the latter two applications, the QM/MM calculations also covered photoinduced processes, namely the excited-state isomerization in HcRed via torsions around the two bridging bonds [39] and the competition between radiationless deactivation and photoadduct formation in photoreceptors with different flavin chromophores [72].

QM/MM techniques have also been used to address solvation effects. Concerning the modeling of zwitterions in water, we have studied the conformations and relative

stabilities of the folded and extended forms of 3-fluoro-γ-aminobutyric acid (FGABA) using discrete microsolvated QM models, a QM/MM treatment of FGABA in TIP3P water, and a standard continuum solvation treatment (PCM). Among these approaches, only the QM/MM free energy calculations gave results consistent with the experimental findings deduced from NMR spectroscoscopy [23]. As part of a study on the photochemical steps in the prebiotic synthesis of precursors from HCN, we used QM/MM MD simulations to estimate the time needed to dissipate the energy of a particular hot ground-state HCN tetramer into the solvent (water), which resulted in a very short time window for the occurrence of hot ground-state reactions during the synthesis [68]. Further ground-state QM/MM MD simulations were carried out to model proton transfer in water [66] and kinetic isotope effects in DHFR [20].

The ChemShell software that has been used in all these applications is available under a license agreement (see www.chemshell.org).

2.5.5 Research Area "Photoinduced Processes in Organic Molecules" (M. Barbatti)

Involved: R. Crespo-Otero, D. Asturiol, D. Mancini

Objective: After UV photoexcitation, organic molecules relax through a manifold of excited states, dissipating the absorbed energy either by photoemission or by vibrational excitation. The objective of this research area is to determine the relaxation mechanisms in two classes of organic systems: a) molecules playing roles in living organisms and b) molecules with potential application as photo-triggers. This goal is accomplished by computational simulations of excited-state dynamics, of potential-energy pathways, and of absorption and emission spectra.

Results:

a) Photophysics of life

Over the past few years, we have investigated the effect of UV radiation on nucleic acid fragments (nucleobases and backbone models) using computational chemistry. This is a topic of major interest as it allows understanding the role played by photochemistry in the biosphere and how carcinogenic and mutagenic effects are induced by radiation. Between 2011 and 2013, we have completed the mapping of the excited-state reaction pathways of cytosine, guanine and uracil (collaboration with H. Lischka). Dynamics simulations for these nucleobases on the ultrafast time-scale revealed that several reaction paths are activated and compete with each other to determine the fate of the reaction. Additionally, we showed that the ionization potentials of adenine along the main reaction paths undergo strong variations that are usually not taken into account either in experimental or in computational analysis (collaboration with S. Ullrich).

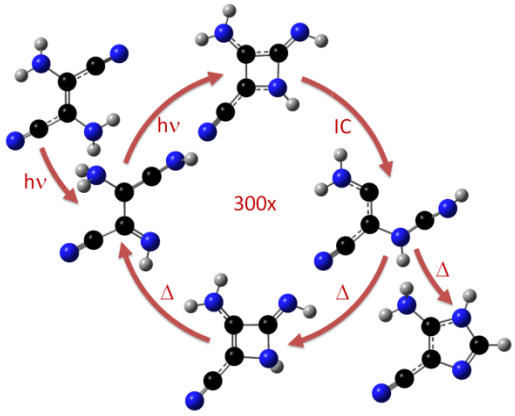

Figure 7. Photochemical steps for synthesis of an imidazole derivative from HCN.

We also investigated the photochemical step of one of the most likely pathways explaining the prebiotic origin of nucleotides on Earth (collaboration with W. Thiel and A. Anoop). This step consists of the photoinduced conversion of a HCN oligomer into an imidazole derivative. Although this photoreaction is known since the 1960s and most current prebiotic models are based on it, the exact reaction mechanism had still not been elucidated. Using dynamics, chemical kinetics, and thermodynamics, we showed that the reaction happens through a long sequence of excitations and de-excitations of an azetene derivative (Fig. 7).

Besides DNA, one of the most important UV chromophores in the skin of mammalians is urocanic acid (UA). The photophysics of this molecule is especially relevant because its *trans-cis* photoisomerization is a main factor inducing skin cancer. Another remarkable feature of UA is that its photoisomerization quantum yield decreases at short wavelengths. Although a number of models based on the topography of the excited-state potential energy surfaces have been proposed to explain this anomalous photophysics, none of them is completely satisfactory. We approached the problem in a distinct way, working under the hypothesis that the anomalous photophysics is caused by tautomeric effects. In fact, spectrum simulations of the tautomers allowed us to show that their relative spectral shift could be the cause of the anomalous photophysics.

A central process in photodynamic therapy is the generation of singlet oxygen ($^1O_2$) by a photosensitizer bound to a carcinogenic cell. Since the 1980s, porphycene (P_C) has been examined as a potentially efficient photosensitizer. We have investigated the UV absorption of P_C and the photophysics of $^1O_2$ generation via P_C sensitization. We showed that 1) there are several $^1O_2$-generation mechanisms available; that 2) the dominant mechanism is dependent on the O_2 concentration; and that 3) highly efficient $^1O_2$ generation could be obtained by encapsulating P_C and O_2 together, opening new conceptual perspectives for photodynamic therapy based on P_C.

As a last point in this research topic, we investigated the photodynamics of two simple models of molecules relevant for biological processes: the N-methyl-formamide (NMF), a model for peptide bonds; and methyl-pentadieniminium cation (Me-PSB3), a model for retinal. In both cases, ultrafast dynamics was simulated using QM/MM methods to incorporate environment effects. In the case of NMF, we showed that a caging effect enables the occurrence of reactions such as proton transfer, which are absent in the gas phase (collaboration with W. Sander). In the case of Me-PSB3, we showed that interaction with a polar solvent changes the orientation of the potential-energy

intersection cone from sloped to peaked, considerably enhancing the speed of deactivation to the ground state.

b) Molecular photo-triggers

Photo-triggers are often used for activation of molecular machines and electronic devices. They work in different ways, for instance, by inducing structural changes via isomerization or dissociation, or by promoting electronic changes via charge transport. We have been investigating a number of different photo-triggers from these two classes. Azobenzene, azomethane, ethylene, and $Cr(CO)_6$ are examples of the first class of photo-triggers. After irradiation, these molecules undergo strong structural changes, which may be communicated to neighboring molecular groups to trigger a reaction. We have simulated the photoinduced ultrafast dynamics of these molecules. In the case of azobenzene, where two nonequivalent rotational pathways corresponding to clockwise or counterclockwise rotations are available, we determined that the course of the rotational motion is strongly dependent on the initial conditions. In fact, we could even demonstrate that the occurrence of one or another pathway can be completely controlled by selecting adequate initial conditions (collaboration with J. Pittner). In the case of $Cr(CO)_6$, dynamics results were used to assign experimental time-constants corresponding to the dissociative motion through the manifold of excited states.

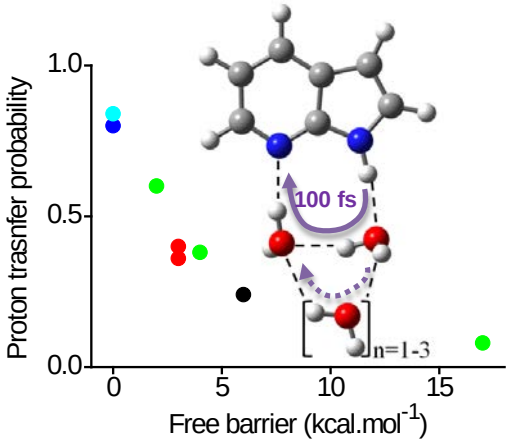

Figure 8. Excited-state intramolecular proton transfer in 7AI-water clusters.

Photoinduced excited-state intramolecular proton transfer in 7-azaindole (7AI), 2-(2´-hydroxyphenyl)benzothiazole and 1H-pyrrolo[3,2-h]quinoline are examples of the second class of photo-triggers. We have simulated the excited-state ultrafast dynamics of these three molecules within small clusters of water and methanol (collaboration with N. Kungwan). While in the gas phase the proton transfer occurs directly between the donor and acceptor groups of the molecule, within clusters the proton is transferred through the network of hydrogen bonds. For all these cases, we showed that the process

is completed within 100 fs. We also mapped the relative importance of several possible reaction pathways. In 7AI-water clusters, for instance, only the nearest two water molecules participate in the proton transfer, while the others play a passive role (Fig. 8).

Outreach: We have made an effort to communicate our results to a more general public through diverse media. Description of our research lines, main results, and new publications are constantly updated on the group homepage (sgk.mpg.de/private/barbatti). A YouTube channel dedicated to movies showing the results of dynamics simulations is also available (youtube.com/user/mbarbatti). News on our work and other relevant information for our field are delivered through our Twitter account (twitter.com/MarioBarbatti). Outstanding results from our research are communicated to general science popularization media. For this last point, we are supported by Sarah-Lena Gombert, from the press-office of our Institute.

2.5.6 Research Area "Development and Assessment of Methods" (M. Barbatti)

Involved: R. Crespo-Otero, T. Cardozo

Objective: Whereas state-of-the-art computational methods allow reaching chemical accuracy for the ground state, simulations of excited states bear a high level of uncertainty. This is due to the many approximations required to deal with the large density of states and the complicated electronic structures of excited states, while still keeping the simulations computationally affordable. The objectives of this research area are a) to implement new methods and algorithms to improve excited-state simulations within the Newton-X platform and b) to critically assess the quality of the calculations.

Results:

a) The Newton-X platform

Since 2005, we have been designing and developing the Newton-X platform. Newton-X is a collection of programs to perform all steps of excited-state nonadiabatic dynamics simulations, from the generation of initial conditions to the statistical analysis. The project involves collaborations with H. Lischka, J. Pittner, G. Granucci, and M. Persico. Newton-X is an open-source platform distributed free of charge. Within the last 12 months (as of October 15, 2013), 150 new downloads have been registered.

Most of new methodologies developed in our group are incorporated into Newton-X. Between 2011 and 2013, we implemented a general hybrid-gradient interface allowing dynamics with QM/MM and ONIOM approaches. We developed a general method for efficient numerical computation of nonadiabatic couplings and for dynamics using the Local Diabatization method. We also developed new interfaces for nonadiabatic dynamics with MCSCF wavefunctions using GAMESS (collaboration with T. Windus); CC2 and ADC(2) using Turbomole; and TDDFT and TDA using Gaussian 09.

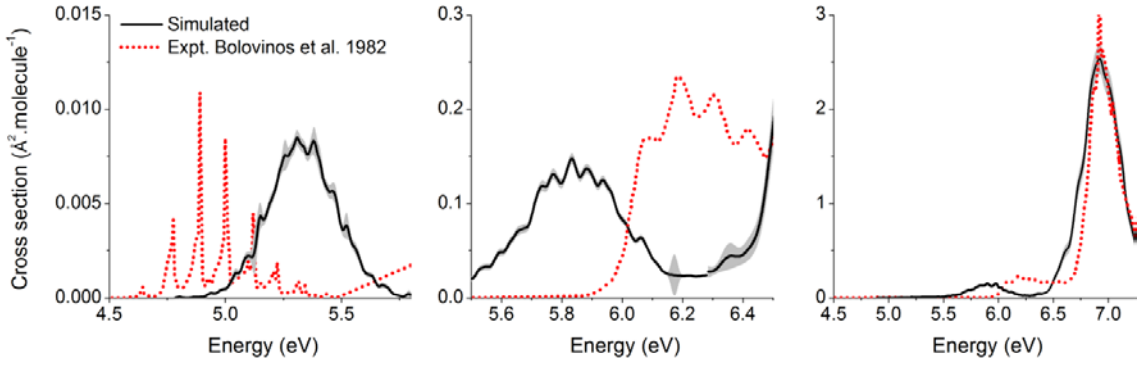

Figure 9. Simulated UV-absorption cross section of 2-phenylfuran compared to experimental results.

State classifications based on CI-type electronic densities were implemented, allowing automatic characterization of the electronic states in terms of local excitations, charge-transfer and delocalized excitations during the dynamics.

Newton-X allows spectrum simulation using ensembles of nuclear geometries. The method can provide absolute intensities, effective parameter-free band widths, and dark vibronic bands (Fig. 9). We presented a formal derivation of the method, which, although popular among several groups, had up to that point only been based on qualitative arguments. This derivation will also allow the development of new algorithms in the future.

b) Method assessment and benchmarks

To understand the impact of the active and reference spaces, we systematically investigated the dynamics of 2-aminopyrimidine at the CASSCF level and of ethylene at the MRCI level (collaboration with H. Lischka). In the first case, we found that the selection of orbitals for the active space has a strong effect on the dynamics output, up to a point where the space is saturated. Before saturation, even with the same nominal number of electrons and orbitals, the dynamics results can be very different for distinct sets of orbitals. After saturation, the results are not affected significantly even when the space is increased. In the case of ethylene, we concluded that the dynamics are influenced not only by the dynamic electron correlation within the π-system, but also within the σ-σ* subsystems and between the σ- and the π-systems. This finding allowed us to explain most of the divergences between simulated and experimental results for the excited-state lifetime of ethylene.

Dynamics simulations for adenine performed with semi-empirical and *ab initio* MRCI predicted similar lifetimes, but deactivation through different pathways. In collaboration with W. Thiel, we systematically repeated these simulations under very controlled conditions. An imbalance in the barriers along two different reaction pathways was found to be the reason for the divergence. Curiously, the imbalance was found in both methods with opposite trends. Under the same conditions, we also tested the dynamics of adenine at the TDDFT level using several functionals. All of them failed to describe the ultrafast dynamics of this molecule. Right now, we are extending these simulations to the ADC(2) level. The collection of all these simulations will provide a useful benchmark of dynamics results for small hetero-aromatic molecules.

We have also validated TDDFT for simulations of donor-acceptor (D-A) interfaces for photovoltaics (collaboration with W. Thiel). Using dimers of thiophene oligomers (D) and fullerene C_{60} (A) as prototypes, we benchmarked the vertical electronic spectra by

systematically changing a number of variables, including oligomer size, density functional (Fig. 10), polarization medium, D-A distance, and chemical functionalization of the monomers. This benchmark will guide the selection of models and computational levels in our future investigations in this field.

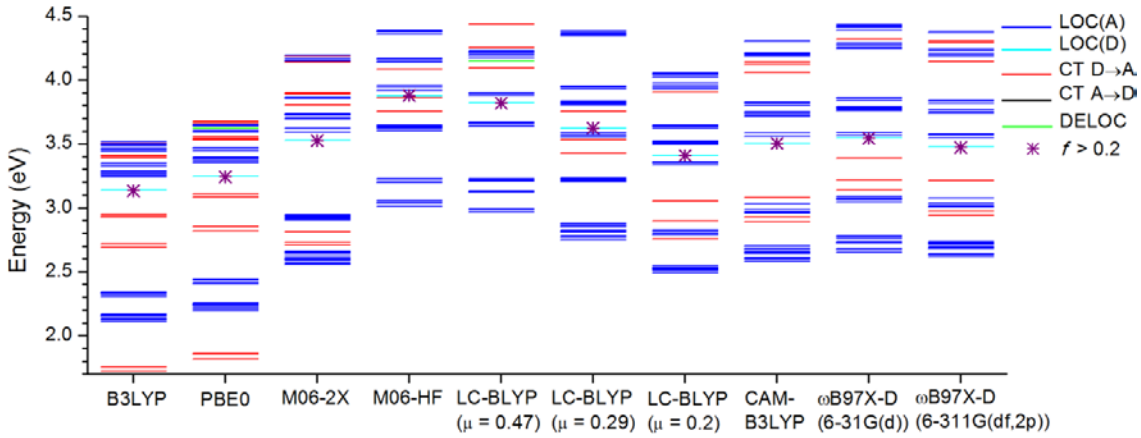

Figure 10. Benchmark of vertical excitations for a thiophene-oligomer/fullerene interface at different levels.

Outreach: Our group supervises the release and distribution of the Newton-X platform. This is done via the Newton-X webpage (www.newtonx.org), where full documentation and tutorials can be accessed. Moreover, we moderate a discussion list at goo.gl/G0H9fg, where a knowledge database is built from users and developers contributions.

2.5.7 Research Area "Molecular Interactions in Organic and Biological Systems. Applications and Methodological Implementations" (E. Sánchez-García)

Involved: K. Bravo-Rodriguez, S. Mittal, P. Sokkar, J.M. Ramirez-Anguita

Objectives: Molecular interactions (MIs) play a key role in chemical and biological processes. However, despite the many scientific advances of the last decades, understanding and predicting the effect of MIs in biological systems is still challenging. In our group we develop computational models to help regulate strategically important molecular interactions in biological systems via the rational manipulation of three factors: *1. the introduction of ligands able to alter protein function, 2. the interactions of proteins with their biological environment,* and *3. the mutagenesis of key residues.* In addition, we also investigate molecular interactions in small model systems like reactive intermediates and closed-shell molecules as a basis to understand more complex systems (Figure 11). One important goal of our research is to predict improved therapeutic agents and approaches, for example in the context of neurodegenerative diseases and the development of new antibiotics.

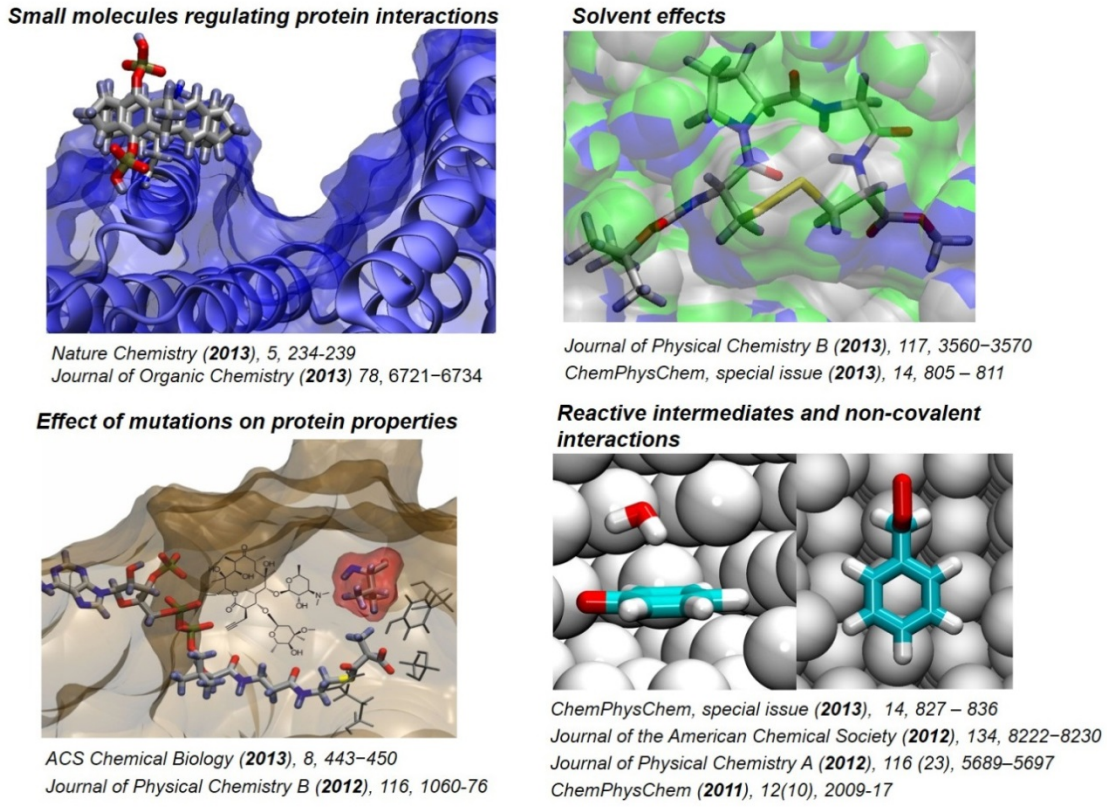

Figure 11. Main research lines and selected representative publications of our group in the last two years.

On the methodological side, we work on generalizing the combination of quantum mechanics (QM) and atomistic molecular mechanics (MM) into a triple-layer QM/MM/CG modeling approach by implementing coarse grained (CG) force fields in the ChemShell code. The aim is to extend the applicability of QM/MM computations to enable an efficient and realistic theoretical treatment of complex chemical, photochemical, and biochemical systems that are challenging for the existing computational methods.

Results:

Molecular interactions in organic and biological systems. Applications

a) Ligands for the regulation of protein properties

Ligands can be used to regulate protein aggregation, enzymatic activity, lipid attachment, and protein–protein interactions, among other important biological properties. In my group we investigate the effect of highly selective ligands such as molecular tweezers (MT) that bind specifically to lysine and arginine, as well as the effect of less specific molecules like aromatic heterocyclic derivatives.

Experimental studies have shown that MTs are able to inhibit the aggregation of Aβ (amyloidogenic peptide related to Alzheimer disease) and IAPP (islet amyloid polypeptide, related to type II diabetes mellitus) without toxic effects, which makes them promising candidates for drug development. In this context, we recently studied the binding mode of four water-soluble tweezers bearing phosphate, phosphonate, sulfate, or O-methylenecarboxylate groups at the central benzene bridge to amino acids and peptides containing lysine or arginine residues. The comparison between experimental and theoretical data provided clear evidence for the unique threading mechanism and the modulating effect of each anion on the interaction of the MTs with positively charged amino acids and peptides. These findings were explained on the basis of the host-guest complex structures obtained from molecular dynamics (MD) simulations and QM/MM methods [120].

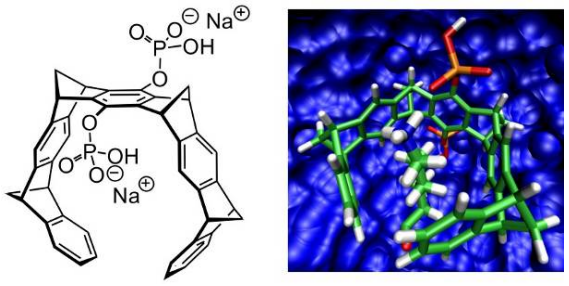

Figure 12. Bishydrogenphosphate tweezer CLR01 (left), CLR01 interacting with lysine, structure optimized in explicit water environment at the QM/MM level (right).

To answer the question of how the tweezers behave in the presence of complex systems with multiple lysine residues, we also studied the effect of molecular tweezers on proteins. We established that molecular tweezers are a powerful tool for regulating 14-3-3 protein-protein interactions for the 14-3-3 σ isoform via an entirely new interference mechanism. Furthermore, the combination of structural analysis and computer modeling allowed us to establish *general rules* for predicting the relative strength and type of interaction of the tweezers with lysine residues in 14-3-3 proteins [118]. We are currently investigating the effect of molecular tweezers on other protein hosts.

Importantly, the study of the interaction motifs and mechanisms of small molecules with several peptide and protein hosts allows us not only to answer important questions related to these systems, but also to guide the design of improved ligands able to reach specific protein regions of biological relevance.

b) Reactive intermediates and synthetic cyclic peptides. Solvent effects

Given the importance of radicals and radical reactions in such diverse aqueous environments as biological systems or tropospheric clouds, it is highly desirable to understand the influence of water and other solvents on their chemical and physical properties. Since we are interested in using molecular interactions with the environment to tune the properties of chemical and biological systems, we study the effect of solvents on reactive intermediates (e.g., radicals) using QM, MD, and QM/MM techniques.

We investigated the complexes of phenoxyl, anilinyl, and benzyl radicals with water using QM and QM/MM MD approaches [53,116]. The influence of molecular interactions on the properties of other model systems like furan complexes [9,115] was also addressed.

Cyclic polypeptides containing a photocleavable disulfide (S-S) bridge are useful models for the study of dynamical conformational changes that convert a polypeptide chain into a three-dimensional protein structure. The conformers of a series of cyclic peptides Cys-Pro-X-Cys (X: Gly, D-Leu, L-Leu, D-Val, L-Val) were studied in the gas phase and in the solvents water and acetonitrile, using both classical MD simulations and QM/MM approaches. We elucidated the effect of the stereochemistry of just a single residue on the conformation of the peptide and on solvent–peptide interactions, and found that the solvent plays a key role for the structural and spectroscopic properties of such systems [119,120].

c) Designed mutagenesis for the regulation of enzymatic activity

Quite often, mutations have deleterious effects and dramatically alter the properties of biological systems. On the other hand, mutations are essential for evolution; and controlled mutagenesis is an important tool to selectively manipulate protein properties. Hence, mutations can be used to regulate photochemical processes, protein folding, protein-protein interactions, and enzymatic activity, among others. Computer simulations play a key role for the molecular understanding and prediction of the effect of mutations.

In our work on *computational mutagenesis*, we aim at providing a molecular understanding of the effect of mutations in biological systems and at delivering computational predictions of targeted mutations able to modify protein properties. Hence, we have investigated disease-associated mutations in rhodopsin [25,121] and the effect of mutations on structural properties of other complex systems. Of especial interest to us are Polyketide Synthases (PKS), which are multienzyme complexes able to direct the formation of a diverse array of functional groups and stereocenters. They catalyze a cascade of Claisen condensations between the enzyme acyl thioester and malonic acid thioesters, which serve as extender units of a nascent polyketide chain. The complex process of extender unit building block selection and incorporation in PKS is mainly controlled by acyltransferase (AT) domains, which catalyze the malonylation of acyl carrier proteins (ACP). A promising option to modify building block specificity in PKS is the direct engineering of innate AT domains to alter their substrate scope by replacing selected amino acids instead of whole catalytic domains.

My group developed computational models for the last acyltransferase domain (AT6) of 6-Desoxyerythronolide B Synthase (DEBS), the key multienzyme complex in the biosynthesis of the antibiotic Erythromycin, to provide a molecular understanding of the effect of directed mutations and the role of specific residues on the enzymatic activity. We were able not only to *rationalize* the effect of point mutations on enzymatic activity, but also to successfully *predict* which single mutation would result in the incorporation of non-native building blocks [117]. The combination of experimental sequence-function correlations (cooperation with F. Schulz) and computational modeling revealed the origins of substrate recognition in PKS domains and enabled their targeted mutagenesis. We are currently extending this research to other systems like monensin PKS (cooperation with F. Schulz).

Implementation of coarse-grained methods in ChemShell

Hybrid QM/MM methods have widespread applications to model biomolecular, organic, inorganic, and organometallic systems with explicit solvation. ChemShell is a QM/MM modular package that allows the combination of several QM and MM methods. Currently, there is considerable interest in the development of coarse-grained (CG) force fields to improve the performance and sampling in MD simulations and geometry optimizations. The CG methodology has been successfully applied to very large molecular systems (such as virus capsids), which are cumbersome to handle at the atomistic level. However, CG approaches do not allow the study of fine structural details (such as fluctuations in secondary structures) due to their approximate representation. To circumvent this problem, hybrid coarse-grained / fine-grained (CG/FG) simulation protocols have been developed.

We work on the implementation of CG force fields in the ChemShell package (cooperation with W. Thiel). By developing novel triple-layer QM/MM/CG modeling approaches, we want to extend the applicability of QM/MM computations. This scheme allows us to treat the chemically important region at the QM level, the area around the QM region at the atomistic MM level, and the rest of the outer region (far from the QM site) at the CG level. In this approach, the presence of the CG region partially eliminates artifacts that may arise from the truncation of the MM region in very large systems. For instance, to study a membrane protein, the lipid bilayer and bulk water may be represented at the CG level while the more important regions are treated at higher resolution. Introducing a CG layer will also reduce the costs of MD simulations. This is especially helpful for QM/MM MD simulations that are currently computationally very expensive, even for smaller systems. Thus, the multi-scale QM/MM/CG approach can also be conveniently used to investigate chemical reactions in explicit solvent, with the bulk solvent being treated at the CG level.

At present, we have already developed a module for the ChemShell code that performs hybrid QM/MM/CG calculations with Martini CG water for the CG layer; we continue this work to include other systems and force fields in our implementation.

2.5.8 Publications 2011-2013 from the Department of Theory

Thiel group

(1) Kumar, D.; Altun, A.; Shaik S.; Thiel, W. *Faraday Discuss.* **2011**, *148*, 373-383.
(2) Benighaus, T.; Thiel, W. *J. Chem. Theory Comput.* **2011**, *7*, 238-249.
(3) Hsiao, Y.-W.; Thiel, W. *J. Phys. Chem. B* **2011**, *115*, 2097-2106.
(4) Kumar, D.; Thiel, W.; de Visser, S. P. *J. Am. Chem. Soc.* **2011**, *133*, 3869-3882.
(5) Metz, S.; Thiel, W. *Coord. Chem. Rev.* **2011**, *255*, 1085-1103.
(6) Weingart, O.; Lan, Z.; Koslowski, A.; Thiel, W. *J. Phys. Chem. Lett.* **2011**, *2*, 1506-1509.
(7) Yachmenev, A.; Yurchenko, S. N.; Jensen, P.; Thiel, W. *J. Chem. Phys.* **2011**, *134*, 244307/1-11.
(8) Lan, Z.; Lu, Y.; Fabiano, E.; Thiel, W. *ChemPhysChem* **2011**, *12*, 1989-1998.
(9) Metzelthin, A.; Sánchez-García, E.; Birer, Ö.; Schwaab, G.; Thiel, W.; Sander W.; Havenith, M. *ChemPhysChem* **2011**, *12*, 2009-2017.
(10) Kazaryan, A.; Lan, Z.; Schäfer, L. V.; Thiel, W.; Filatov, M. *J. Chem. Theory Comput.* **2011**, *7*, 2189-2199.
(11) Lu, Y.; Lan, Z.; Thiel, W. *Angew. Chem., Int. Ed.* **2011**, *50*, 6864-6867.
(12) Yachmenev, A.; Yurchenko, S. N.; Ribeyre, T.; Thiel, W. *J. Chem. Phys.* **2011**, *135*, 074302/1-13.
(13) Breidung, J.; Thiel, W. *In Handbook of High-Resolution Spectroscopies*, vol. 1; Quack, M.; Merkt, F., Eds.; Wiley: Chichester, UK, 2011; pp. 389-404.
(14) Fabiano, E.; Lan, Z.; Lu, Y.; Thiel, W. In *Conical Intersections: Theory, Computation and Experiment*; Domcke, W.; Yarkony, D. R.; Köppel ,H., Eds.; World Scientific Publishing: Singapore, 2011; chapter 12, pp. 463-496.
(15) Yurchenko, S. N.; Barber, R. J.; Tennyson, J.; Thiel, W.; Jensen, P. *J. Mol. Spectrosc.* **2011**, *268*, 123-129.
(16) Inés, B.; Patil, M.; Carreras, J.; Goddard, R.; Thiel, W.; Alcarazo, M. *Angew. Chem., Int. Ed.* **2011**, *50*, 8400-8403.
(17) Korth, M.; Thiel, W. *J. Chem. Theory Comput.* **2011**, *7*, 2929-2936.
(18) Meletis, P.; Patil, M.; Thiel, W.; Frank, W.; Braun, M. *Chem. Eur. J.* **2011**, *17*, 11243-11249.
(19) Thiel, W. *Angew. Chem., Int. Ed.* **2011**, *50*, 9216-9217.
(20) Doron, D.; Major, D. T.; Kohen, A.; Thiel, W.; Wu, X. *J. Chem. Theory Comput.* **2011**, *7*, 3420-3437.
(21) Ramalho, T. C.; Pereira, D. H.; Thiel, W. *J. Phys. Chem. A* **2011**, *115*, 13504-13512.
(22) Petůskova, J.; Patil, M.; Holle, S.; Lehmann, C. W.; Thiel, W.; Alcarazo, M. *J. Am. Chem. Soc.* **2011**, *133*, 20758-20760.
(23) Cao, J.; Bjornsson, R.; Bühl, M.; Thiel, W.; van Mourik, T. *Chem.–Eur. J.* **2012**, *18*, 184-195.

(24) Cui, G.; Lan, Z.; Thiel, W. *J. Am. Chem Soc.* **2012**, *134*, 1662-1672.
(25) Hernández-Rodríguez, E. W.; Sánchez-García, E.; Crespo-Otero, R.; Montero-Alejo, A. L.; Montero, L. A.; Thiel, W. *J. Phys. Chem. B* **2012**, *116*, 1060-1076.
(26) Meier, K.; Thiel, W.; van Gunsteren, W. F. *J. Comput. Chem.* **2012**, *33*, 363-378.
(27) Polyak, I.; Reetz, M. T.; Thiel, W. *J. Am. Chem. Soc.* **2012**, *134*, 2732-2741.
(28) Lan, Z.; Lu, Y.; Weingart, O.; Thiel, W. *J. Phys. Chem. A* **2012**, *116*, 1510-1518.
(29) Gómez, H.; Polyak, I.; Thiel, W.; Lluch, J. M.; Masgrau, L. *J. Am. Chem. Soc.* **2012**, *134*, 4743-4752.
(30) Lu, Y.; Lan, Z.; Thiel, W. *J. Comput. Chem.* **2012**, *33*, 1225-1235.
(31) Cui, G.; Lu, Y.; Thiel, W. *Chem. Phys. Lett.* **2012**, *537*, 21-26.
(32) Heggen, B.; Lan, Z.; Thiel, W. *Phys. Chem. Chem. Phys.* **2012**, *14*, 8137-8146.
(33) Wu, X.; Koslowski, A.; Thiel, W. *J. Chem. Theory Comput.* **2012**, *8*, 2272-2281.
(34) Gámez, J. A.; Weingart, O.; Koslowski, A.; Thiel, W. *J. Chem. Theory Comput.* **2012**, *8*, 2352-2358.
(35) Barbatti, M.; Lan, Z.; Crespo-Otero, R.; Szymczak, J. J.; Lischka, H.; Thiel, W. *J. Chem. Phys.* **2012**, *137*, 22A503/1-14.
(36) Hsiao, Y.-W.; Götze, J.; Thiel, W. *J. Phys. Chem. B* **2012**, *116*, 8064-8073.
(37) Patil, M.; Thiel, W. *Chem.–Eur. J.* **2012**, *18*, 10408-10418.
(38) Liao, R.-Z.; Thiel, W. *J. Phys. Chem. B.* **2012**, *116*, 9396-9408.
(39) Sun, Q.; Li, Z.; Lan, Z.; Pfisterer, C.; Doerr, M.; Fischer, S.; Smith, S. C.; Thiel, W. Phys. *Chem. Chem. Phys.* **2012**, *14*, 11413-11424.
(40) Schönborn, J. B.; Koslowski, A.; Thiel, W.; Hartke, B. *Phys. Chem. Chem. Phys.* **2012**, *14*, 12193-12201.
(41) Cui, G.; Thiel, W. *Phys. Chem. Chem. Phys.* **2012**, *14*, 12378-12384.
(42) Teller, H.; Corbet, M.; Mantilli, L.; Gopakumar, G.; Goddard, R.; Thiel, W.; Fürstner, A. *J. Am. Chem. Soc.* **2012**, *134*, 15331-15342.
(43) Liao, R.-Z.; Thiel, W. *J. Chem. Theory Comput.* **2012**, *8*, 3793-3803.
(44) Carreras, J.; Patil, M.; Thiel, W.; Alcarazo, M. *J. Am. Chem. Soc.* **2012**, *134*, 16753-16758.
(45) Saito, T.; Thiel, W. *J. Phys. Chem. A* **2012**, *116*, 10864-10869.
(46) Boulanger E.; Thiel, W. *J. Chem. Theory Comput.* **2012**, *8*, 4527-4538.
(47) Yurchenko, S. N.; Thiel, W.; Jensen, P. *AIP Conf. Proc.* **2012**, *1504*, 491-494.
(48) Cui, G.; Thiel, W. *Angew. Chem., Int. Ed. 52*, **2013**, 433-436.
(49) Sen, K.; Crespo-Otero, R.; Weingart, O.; Thiel, W.; Barbatti, M. *J. Chem. Theory Comput.* **2013**, *9*, 533-542.
(50) Grebner, C.; Kästner, J.; Thiel, W.; Engels, B. *J. Chem. Theory Comput.* **2013**, *9*, 814-821.
(51) Liao, R.-Z.; Thiel, W. *J. Phys. Chem. B* **2013**, *117*, 1326-1336.
(52) Čorić, I.; Kim, J. H.; Vlaar, T.; Patil, M.; Thiel, W.; List, B. *Angew. Chem., Int. Ed.* **2013**, *52*, 3490-3493.

(53) Crespo-Otero, R.; Bravo-Rodriguez, K.; Roy, S.; Benighaus, T.; Thiel, W.; Sander, W.; Sánchez-García, E. *ChemPhysChem* **2013**, *14*, 805-811.
(54) Kozma, Á.; Gopakumar, G.; Farès, C.; Thiel, W.; Alcarazo, M. *Chem.–Eur. J.* **2013**, *19*, 3542-3546.
(55) Götze, J. P.; Thiel, W. *Chem. Phys.* **2013**, *415*, 247-255.
(56) Patil, M.; Loerbroks, C.; Thiel, W. *Org. Lett.* **2013**, *15*, 1682-1685.
(57) Liao, R.-Z.; Thiel, W. *J. Phys. Chem. B* **2013**, *117*, 3954-3961.
(58) Lifchits, O.; Mahlau, M.; Reisinger, C. M.; Lee, A.; Farès, C.; Polyak, I.; Gopakumar, G.; Thiel, W.; List, B. *J. Am. Chem. Soc.* **2013**, *135*, 6677-6693.
(59) Polyak, I.; Reetz, M. T.; Thiel, W. *J. Phys. Chem. B 117*, **2013**, 4993-500.
(60) Khan, S.; Gopakumar, G.; Thiel, W.; Alcarazo, M. *Angew. Chem., Int. Ed.* **2013**, *52*, 5644-5647.
(61) Huang, X.; Patil, M.; Farès, C.; Thiel, W.; Maulide, N. *J. Am. Chem. Soc.* **2013**, *135*, 7312-7323.
(62) Kumari, D.; Singh, H.; Patil, M.; Thiel, W.; Pant, C. S.; Banerjee, S. *Thermochim. Acta* **2013**, *562*, 96-104.
(63) Fortenberry, R. C.; Huang, X.; Yachmenev, A.; Thiel, W.; Lee, T. J. *Chem. Phys. Lett.* **2013**, *574*, 1-12.
(64) Audisio, D.; Gopakumar, G.; Xie, L.-G.; Alves, L. G.; Wirtz, C.; Martins, A. M.; Thiel, W.; Farès, C.; Maulide, N. *Angew. Chem., Int. Ed.* **2013**, *52*, 6313-6316.
(65) Spörkel, L.; Cui, G.; Thiel, W. *J. Phys. Chem. A* **2013**, *117*, 4574-4583.
(66) Wu, X.; Thiel, W.; Pezeshki, S.; Lin, H. *J. Chem. Theory Comput.* **2013**, *9*, 2672-2686.
(67) Gámez, J. A.; Weingart, O.; Koslowski, A.; Thiel, W. *Phys. Chem. Chem. Phys.* **2013**, *15*, 11814-11821.
(68) Boulanger, E.; Anoop, A.; Nachtigallova, D.; Thiel, W.; Barbatti, M. *Angew. Chem., Int. Ed.* **2013**, *52*, 8000-8003.
(69) Polyak, I.; Boulanger, E.; Sen, K.; Thiel, W. *Phys. Chem. Chem. Phys.* **2013**, *15*, 14188-14195.
(70) Polyak, I.; Benighaus, T.; Boulanger, E.; Thiel, W. *J. Chem. Phys.* **2013**, *139*, 064104/1-11.
(71) Marquardt, R.; Sagui, K.; Zheng, J.; Thiel, W.; Luckhaus, D.; Yurchenko, S.; Mariotti, F.; Quack, M. *J. Phys. Chem. A* **2013**, *117*, 7502-7522.
(72) Silva-Junior, M. R.; Mansurova, M.; Gärtner, W.; Thiel, W. *ChemBioChem* **2013**, *14*, 1648-1661.
(73) Karasulu, B.; Patil, M.; Thiel, W. *J. Am. Chem. Soc.* **2013**, *135*, 13400-13413.
(74) Cui, G.; Cao, X.-Y.; Fang, W.-H.; Dolg, M.; Thiel, W. *Angew. Chem., Int. Ed.* **2013**, *52*, 10281-10285.
(75) Liao, R.-Z.; Thiel, W. *J. Comput. Chem.* **2013**, *34*, 2389-2397.
(76) Yurchenko, S. N.; Tennyson, J.; Barber, R. J.; Thiel, W. *J. Mol. Spectrosc.* **2013**, *291*, 69-76.

(77) Escudero, D.; Heuser, E.; Meier, R. J.; Schäferling, M.; Thiel, W.; Holder, E. *Chem.–Eur. J.* **2013**, *19*, 15639-15644.
(78) Loerbroks, C.; Rinaldi, R.; Thiel, W. *Chem.–Eur. J.* **2013**, *19*, 16282-16294.
(79) Thiel, W. *Nachr. Chem.* **2013**, *61*, 1095-1096.
(80) Thiel, W.; Hummer, G. *Nature* **2013**, *504*, 96-97.
(81) Yachmenev, A.; Polyak, I.; Thiel, W. *J. Chem. Phys.* **2013**, *139*, 204308/1-14.
(82) Götze, J. P.; Karasulu, B.; Thiel, W. *J. Chem. Phys.* **2013**, *139*, 234108/1-8.
(83) Carreras, J.; Gopakumar, G.; Gimeno, A.; Linowski, P.; Petuškova, J.; Thiel, W.; Alcarazo, M. *J. Am. Chem. Soc.* **2013**, *135*, 18815-18823.
(84) Seidel, G.; Gabor, B.; Goddard, R.; Heggen, B.; Thiel, W.; Fürstner, A. *Angew. Chem., Int. Ed.* **2014**, *53*, 879-882.

Barbatti group

(35) Barbatti, M.; Lan, Z.; Crespo-Otero, R.; Szymczak, J. J.; Lischka, H.; Thiel, W. *J. Chem. Phys.* **2012**, *137*, 22A503/1-14.
(49) Sen, K.; Crespo-Otero, R.; Weingart, O.; Thiel, W.; Barbatti, M. *J. Chem. Theory Comput.* **2013**, *9*, 533-542.
(68) Boulanger, E.; Anoop, A.; Nachtigallova, D.; Thiel, W.; Barbatti, M. *Angew. Chem., Int. Ed.* **2013**, *52*, 8000-8003.
(85) Barbatti, M. *WIREs: Comp. Mol. Sci.* **2011**, *1*, 620-633.
(86) Barbatti, M. *Phys. Chem. Chem. Phys.* **2011**, *13*, 4686-4692.
(87) Barbatti, M.; Aquino, A. J. A.; Szymczak, J. J.; Nachtigallová, D.; Lischka, H. *Phys. Chem. Chem. Phys.* **2011**, *13*, 6145-6155.
(88) Barbatti, M.; Szymczak, J. J.; Aquino, A. J. A.; Nachtigallová, D.; Lischka, H. *J. Chem. Phys.* **2011**, *134*, 014304/1-5.
(89) Barbatti, M.; Ullrich, S. *Phys. Chem. Chem. Phys.* **2011**, *13*, 15492-15500.
(90) Crespo-Otero, R.; Barbatti, M. *J. Chem. Phys.* **2011**, *134*, 164305/1-12.
(91) Crespo-Otero, R.; Barbatti, M.; Yu, H.; Evans, N. L.; Ullrich, S. *ChemPhysChem* **2011**, *12*, 3365-3375.
(92) Daengngern, R.; Kungwan, N.; Wolschann, P.; Aquino, A. J. A.; Lischka, H.; Barbatti, M. *J. Phys. Chem. A* **2011**, *115*, 14129-14136.
(93) Barbatti, M.; Shepard, R.; Lischka, H. In *Conical Intersections*; Domcke, W.; Yarkony, D. R.; Koppel, H., Eds.; Singapore: World Scientific, 2011; pp. 415-462.
(94) Nachtigallová, D.; Aquino, A. J. A.; Szymczak, J. J.; Barbatti, M.; Hobza, P.; Lischka, H. *J. Phys. Chem. A* **2011**, *115*, 5247-5255.
(95) Pederzoli, M.; Pittner, J.; Barbatti, M.; Lischka, H. *J. Phys. Chem. A* **2011**, *115*, 11136-11143.
(96) Szalay, P. G.; Aquino, A. J. A.; Barbatti, M.; Lischka, H. *Chem. Phys.* **2011**, *380*, 9-16.

(97) Szymczak, J. J.; Barbatti, M.; Lischka, H. *Int. J. Quantum Chem.* **2011**, *111*, 3307-3315.
(98) Barbatti, M.; Nascimento, M. A. C. *Int. J. Quantum Chem.* **2012**, *112*, 3169-3173.
(99) Barbatti, M.; Ruckenbauer, M.; Szymczak, J.; Sellner, B.; Vazdar, M.; Antol, I.; Eckert-Maksić, M.; Lischka, H. In *Handbook of Computational Chemistry*; Leszczynski, J., Ed.; Dordrecht: Springer Science+Business Media B.V., 2012; pp. 1175-1213.
(100) Borges, I.; Barbatti, M.; Aquino, A. J. A.; Lischka, H. *Int. J. Quantum Chem.* **2012**, *112*, 1225-1232.
(101) Crespo-Otero, R.; Barbatti, M. *Theor. Chem. Acc.* **2012**, *131*, 1237.
(102) Homem, M. G. P.; Lopez-Castillo, A.; Barbatti, M.; Rosa, L. F. S.; Iza, P.; Cavasso-Filho, R. L.; Farenzena, L. S.; Lee, M. T.; Iga I. *J. Chem. Phys.* **2012**, *137*, 184305/1-9.
(103) Kungwan, N.; Plasser, F.; Aquino, A. J. A.; Barbatti, M.; Wolschann, P.; Lischka, H. *Phys. Chem. Chem. Phys.* **2012**, *14*, 9016-9025.
(104) Lan, Z.; Nonell, S.; Barbatti, M. *J. Phys. Chem. A* **2012**, *116*, 3366-3376.
(105) Pederzoli, M.; Pittner, J.; Barbatti, M.; Lischka, H. *Proc. SPIE* **2012**, *8463*, 846318.
(106) Plasser, F.; Granucci, G.; Pittner, J.; Barbatti, M.; Persico, M.; Lischka, H. *J. Chem. Phys.* **2012**, *137*, 22A514/1-13.
(107) Plasser, F.; Barbatti, M.; Aquino, A.; Lischka, H. *Theor. Chem. Acc.* **2012**, *131*, 1073.
(108) Asturiol, D.; Barbatti, M. *J. Chem. Phys.* **2013**, *139*, 074307/1-7.
(109) Barbatti, M.; Ruckenbauer, M.; Plasser, F.; Pittner, J.; Granucci, G.; Persico, M.; Lischka, H. *WIREs Comp. Mol. Sci.*, DOI:10.1002/wcms.1158.
(110) Crespo-Otero, R.; Mardyukov, A.; Sánchez-García, E.; Barbatti, M.; Sander, W. *ChemPhysChem* **2013**, *14*, 827-836.
(111) Daengngern, R.; Kerdpol, K.; Kungwan, N.; Hannongbua, S.; Barbatti, M. *J. Photochem. Photobiol., A* **2013**, *266*, 28-36.
(112) Kungwan, N.; Daengngern, R.; Piansawan, T.; Hannongbua, S.; Barbatti, M. *Theor. Chem. Acc.* **2013**, *132*, 1397 (1-10).
(113) Ruckenbauer, M.; Barbatti, M.; Müller, T.; Lischka, H. *J. Phys. Chem. A* **2013**, *117*, 2790-2799.
(114) Sellner, B.; Barbatti, M.; Müller, T.; Domcke, W.; Lischka, H. *Mol. Phys.* **2013**, *111*, 2439-2450.

Sánchez-García group

(9) Metzelthin, A.; Sánchez-García, E.; Birer, Ö.; Schwaab, G.; Thiel, W.; Sander W.; Havenith, M. *ChemPhysChem* **2011**, *12*, 2009-2017.

(25) Hernández-Rodríguez, E. W.; Sánchez-García, E.; Crespo-Otero, R.; Montero-Alejo, A. L.; Montero, L. A.; Thiel, W. *J. Phys. Chem. B* **2012**, *116*, 1060-1076.

(53) Crespo-Otero, R.; Bravo-Rodriguez, K.; Roy, S.; Benighaus, T.; Thiel, W.; Sander, W.; Sánchez-García, E. *ChemPhysChem* **2013**, *14*, 805-811.

(110) Crespo-Otero, R.; Mardyukov, A.; Sánchez-García, E.; Barbatti, M.; Sander, W. *ChemPhysChem* **2013**, *14*, 827-836.

(115) Sánchez-García, E.; Jansen, G. *J. Phys. Chem. A* **2012**, *116*, 1060-1076.

(116) Sander, W.; Roy, S.; Polyak, I.; Ramirez-Anguita, J. M.; Sánchez-García, E. *J. Am. Chem. Soc.* **2012**, *134*, 8222-8230.

(117) Sundermann, U.; Bravo-Rodriguez, K.; Klopries, S.; Kushnir, S.; Gomez, H.; Sanchez-Garcia, E.; Schulz, F. *ACS Chem. Biol.* **2013**, *8*, 443-450.

(118) Bier, D.; Rose, R.; Bravo-Rodriguez, K.; Bartel, M.; Ramirez-Anguita, J. M.; Dutt, S.; Wilch, C.; Klärner, F.-G.; Sanchez-Garcia, E.; Schrader, T.; Ottmann, C. *Nat. Chem.* **2013**, *5*, 234-239.

(119) Li, F.; Bravo-Rodriguez, K.; Phillips, C.; Seidel, R. W.; Wieberneit, F.; Stoll, R.; Doltsinis, N. L.; Sanchez-Garcia, E.; Sander, W. *J. Phys. Chem. B* **2013**, *117*, 3560-3570.

(120) Dutt, S.; Wilch, C.; Gersthagen, T.; Talbiersky, P.; Bravo-Rodriguez, K.; Hanni, M.; Sánchez-García, E.; Ochsenfeld, C.; Klärner, F.; Schrader, T. *J. Org. Chem.* **2013**, *78*, 6721-6734.

(121) Hernández-Rodríguez, E. W.; Montero-Alejo, A. L.; López, R.; Sánchez-García, E.; Montero-Cabrera, L. A.; García de la Vega, J. M. *J. Comput. Chem.* **2013**, *34*, 2460-2471.

(122) Li, F.; Bravo-Rodriguez, K.; Fernandez-Oliva, M.; Ramirez-Anguita, J. M.; Merz, K.; Winter, M.; Lehmann, C. W.; Sander, W.; Sánchez-García, E. *J. Phys. Chem. B* **2013**, *117*, 10785-10791.

Publications by Other Members of the Department

(123) **Korth**, M. *ChemPhysChem* **2011**, *12*, 3131-3142.

(124) **Weingart**, O.; Altoe, P.; Stenta, M.; Bottoni, A.; Orlandi, G.; Garavelli, M. *Phys. Chem Chem. Phys.* **2011**, *13*, 3645-3648.

(125) Suardiaz, R.; **Crespo-Otero**, R.; Perez, C.; San Fabian, J.; de la Vega, J. M. G. *J. Chem. Phys.* **2011**, *134*, 061101/1-4.

(126) Ai, Y.-J.; **Liao**, R.-Z.; Fang, W.-H.; Luo, Y. *Phys. Chem. Chem. Phys.* **2012**, *14*, 13409-13414.

(127) **Götze**, J. P.; Greco, C.; Mitrić, R.; Bonačić-Koutecký, V.; Saalfrank, P. *J. Comput. Chem.* **2012**, *33*, 2233-2242.
(128) **Götze**, J. P.; Saalfrank, P. *J. Mol. Model.* **2012**, *18*, 1877-1883.
(129) Klaffki, N.; **Weingart**, O.; Garavelli, M.; Spohr, E. *Phys. Chem Chem. Phys.* **2012**, *14*, 14299-14305.
(130) Kröner, D.; **Götze**, J. P. *J. Photochem. Photobiol. B* **2012**, *109*, 12-19.
(131) Muya, J. T.; **Gopakumar**, G.; Lijnen, E.; Nguyen, M. T.; Ceulemans A. In *Vibronic Interactions and the Jahn-Teller Effect: Theory and Applications*; Atanasov, M.; Daul, C.; Tregenna-Piggott, P., Eds.; Prog. Theor. Chem. Phys., vol. 23; Berlin: Springer, 2012; pp. 265-278.
(132) Nordin, M.; **Liao**, R.-Z.; Ahlford, K.; Adolfsson, H.; Himo, F. *ChemCatChem* **2012**, *4*, 1095-1104.
(133) **Weingart**, O.; Garavelli, M. *J. Chem. Phys.* **2012**, *137*, 22A523/1-6.
(134) Yang, L.; **Liao**, R.-Z.; Ding, W.-J.; Yu, J.-G.; Liu, K.; Liu, R.-Z. *Theor. Chem. Acc.* **2012**, *131*, 1275.
(135) Muya, J. T.; Ramanantoanina, H.; Daul, C.; Nguyen, M. T.; **Gopakumar**, G.; Ceulemans, A. *Phys. Chem. Chem. Phys.* **2013**, *15*, 2829-2835.
(136) de la Vega, J. M. G.; San Fabian, J.; **Crespo-Otero**, R.; Suardiaz, R.; Perez, C. *Int. J. Quantum Chem.* **2013**, *113*, 656-660.
(137) **Liao**, R.-Z. *J. Biol. Inorg. Chem.* **2013**, *18*, 175-181.
(138) Seidel, R. W.; Goddard, R.; **Breidung**, J.; Bamfaste, P.; Neff, D.; Oppel, I. M. *Struct. Chem.* **2013**, *24*, 181-189.
(139) Krasnopolski, M.; Seidel, R. W.; Goddard, R.; **Breidung**, J.; Winter, M. V.; Devi, A.; Fischer, R. A. *J. Mol. Struct.* **2013**, *1031*, 239-245.
(140) Seidel, R. W.; Dietz, C.; **Breidung**, J.; Goddard, R.; Oppel, I. M. *Acta Crystallogr., Sect. C: Cryst. Struct. Commun.* **2013**, *69*, 1112-1115.
(141) Zhang, Z. G.; Roiban, G. D.; Acevedo, J. P.; **Polyak**, I.; Reetz, M. T. *Adv. Synth. Cat.* **2013**, *355*, 99-106.
(142) **Cui**, G.; Fang, W. *J. Chem. Phys.* **2013**, *138*, 044315/1-9.
(143) Goy, R.; Apfel, U.-P.; Elleouet, C.; **Escudero**, D.; Elstner, M.; Görls, H.; Talarmin, J.; Schollhammer, P.; González, L.; Weigand, W. *Eur. J. Inorg. Chem.* **2013**, 4466-4472.

Publications by other members of the Department (marked in bold) are included only if they carry the address of the Institute.

There are seven joint theory papers, which are listed twice but with a unique number.

Joint research projects between the Thiel group and experimental groups in the Institute are documented in fifteen joint publications, which are listed both here and in the section of the experimental partner.